Article

Current Biology

Days-old zebrafish rapidly learn to recognize threatening agents through noradrenergic and forebrain circuits

Highlights

- Larval zebrafish are capable of learned predator recognition
- Learning occurs within ~1 min and as early as 5 days post-fertilization
- Whole-brain functional imaging implicates neuromodulatory and forebrain dynamics
- Ablations suggest that noradrenergic and forebrain circuits mediate learning

Authors

Dhruv Zocchi, Millen Nguyen, Emmanuel Marquez-Legorreta, ..., David A. Prober, Elizabeth M.C. Hillman, Misha B. Ahrens

Correspondence

ahrensm@janelia.hhmi.org

In brief

Zocchi et al. utilize a robotic predator-learning assay to show that larval zebrafish as young as 5 days post-fertilization rapidly learn to avoid robots following predatory-like experiences. Whole-brain imaging of neural activity implicates the noradrenergic system and forebrain populations in this "conditioned robot avoidance" learning.

Zocchi et al., 2025, Current Biology *35*, 1–14
January 6, 2025
https://doi.org/10.1016/j.cub.2024.11.057

CellPress

Current Biology

CellPress

Article

Days-old zebrafish rapidly learn to recognize threatening agents through noradrenergic and forebrain circuits

Dhruv Zocchi,[1] Millen Nguyen,[1] Emmanuel Marquez-Legorreta,[1] Igor Siwanowicz,[1] Chanpreet Singh,[2] David A. Prober,[2] Elizabeth M.C. Hillman,[3] and Misha B. Ahrens[1,4,*]

[1]Janelia Research Campus, Howard Hughes Medical Institute, Ashburn, VA 20147, USA
[2]California Institute of Technology, Division of Biology and Biological Engineering, Pasadena, CA 91125, USA
[3]Columbia University, Mortimer B. Zuckerman Mind Brain Behavior Institute, Departments of Biomedical Engineering and Radiology, New York, NY 10027, USA
[4]Lead contact
*Correspondence: ahrensm@janelia.hhmi.org
https://doi.org/10.1016/j.cub.2024.11.057

SUMMARY

Animals need to rapidly learn to recognize and avoid predators. This ability may be especially important for young animals due to their increased vulnerability. It is unknown whether, and how, nascent vertebrates are capable of such rapid learning. Here, we used a robotic predator-prey interaction assay to show that 1 week after fertilization—a developmental stage where they have approximately 1% the number of neurons of adults—zebrafish larvae rapidly and robustly learn to recognize a stationary object as a threat after the object pursues the fish for ~1 min. Larvae continue to avoid the threatening object after it stops moving and can learn to distinguish threatening from non-threatening objects of a different color. Whole-brain functional imaging revealed the multi-timescale activity of noradrenergic neurons and forebrain circuits that encoded the threat. Chemogenetic ablation of those populations prevented the learning. Thus, a noradrenergic and forebrain multiregional network underlies the ability of young vertebrates to rapidly learn to recognize potential predators within their first week of life.

INTRODUCTION

Survival in challenging environments requires recognizing and avoiding predators. Recognition of familiar conspecifics can rely on a static set of sensory cues that does not change across an animal's lifetime.[1–5] However, the appearance of specific predators can change due to migration or population fluctuations. Therefore, predator avoidance often relies on learned recognition,[6–8] a non-trivial task where the prey must extract and learn features of the predator in the midst of predation. Moreover, because an attack can lead to death, learning must happen rapidly, ideally after a single predator-prey interaction.

Larval zebrafish face the predator recognition problem since they do not receive parental protection. It is unclear whether their ultra-compact brains, containing 100 times fewer neurons than the adult brain,[9–11] can support such rapid learning. While young zebrafish[12,13] and rats[14] can perform some forms of learning, this learning occurs on the timescale of tens of minutes[12–25]: slower and less robustly than in older animals.[12,14,26,27] Thus, it is unknown whether nascent animals can learn at timescales required for predator recognition.

Studies of biological learning have made great strides in describing learning-associated changes at the level of molecules,[28–30] synapses,[31–34] and individual brain regions,[19,35–40] with most studies performed in adult animals. We asked whether very young vertebrates can learn to recognize an otherwise innocuous-looking object as a threat after a very brief display of aggression, and what brain mechanisms enable such rapid learning. We developed a simulated predatory experience,[41–46] called "conditioned robot avoidance" (CRA), where larval zebrafish experience brief negative interactions with robots in their environment. In CRA, a small cylindrical robot starts off inanimate, but then it "comes to life" and begins to move autonomously and chase the fish. We found that within a few minutes of intermittent chases, larvae aged 5–13 days post-fertilization (dpf) learned that the robot posed a threat, and they avoided it for tens of minutes, even when it was no longer moving. This recognition was specific, as a robot of a different color but otherwise identical appearance did not induce avoidance, implying a remarkable ability of the young larvae to not over-generalize the learned avoidance. We found that larvae display learned avoidance toward the robots at a surprisingly young age range at which they still have difficulty with other learning tasks,[12,17] indicating a staggered emergence of associative learning capabilities.

Through whole-brain functional imaging during threat exposure and a screen for involvement of the major neuromodulatory systems, we tracked the neuronal signals underlying the learning to distributed regions of the forebrain and the noradrenergic (NE) system. Response dynamics in forebrain regions, including the habenula[47,48] and telencephalon, were necessary for learning and were functionally coupled to locus coeruleus (LC) dynamics, consistent with a learning mechanism involving LC-driven

Please cite this article in press as: Zocchi et al., Days-old zebrafish rapidly learn to recognize threatening agents through noradrenergic and forebrain circuits, Current Biology (2024), https://doi.org/10.1016/j.cub.2024.11.057

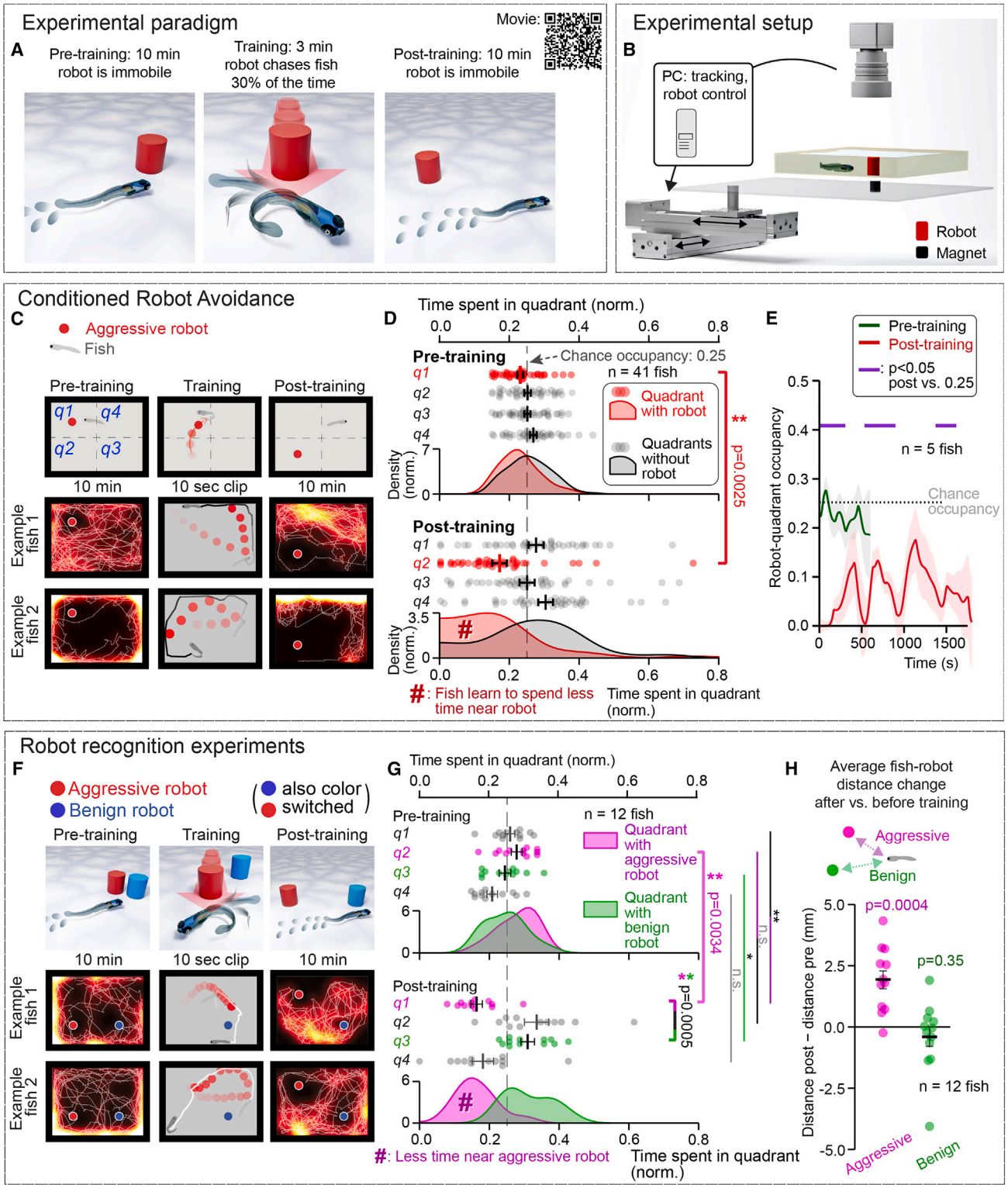

Figure 1. Conditioned robot avoidance learning in larval zebrafish

(A) Schematic of experiment and behavioral effect of conditioned robot avoidance (CRA). Fish does not initially avoid the immobile robot. Following 3 min of intermittent chase by the robot (60–90 s of chase interspersed with random motion), fish avoids robot for tens of minutes. See Figure S1A and Videos S1 and S2 at Mendeley Data: http://www.doi.org/10.17632/wkxwggvfbx.1.

(B) Schematic of the fish-robot interaction behavioral setup (STAR Methods for details).

(legend continued on next page)

signaling to distributed regions of the forebrain. Together, these observations reveal a NE-driven form of rapid predator learning in a nascent vertebrate brain containing just 1% of the number of neurons of its adult counterpart.

RESULTS

Larval zebrafish rapidly learn to recognize objects that are capable of attack

We tested whether larval zebrafish could learn to avoid a simple, stationary physical object after experiencing it as "coming to life" and interacting aggressively with them for a brief period of time (Figures 1A and 1B). The robot, slightly larger than the larva, was designed to look neutral, so that its predator-like attributes had to be learned from aggressive interactions with the fish. Fish swam in an arena (2 cm length, 2.5 cm width, 5 mm depth) in the presence of the robot, which was initially stationary. During 3–4 min of training, the robot chased the fish intermittently, with periods of random motion in between brief chase sequences (total duration of the chases was 60–90 s). Swim behavior was compared pre- and post-training, while the robot was immobile for 10 min in each period (Figures 1A and S1A; Video S1). With this system in place, we tested whether fish could associate the robot with the attributes of a predator-like being, even after the robot stops moving. After the short chase training protocol, in the post-training period we found that most fish avoided the immobile robot, as quantified by measuring time spent in each of the four quadrants of the behavioral arena (Figures 1C and 1D; Video S1). A Gaussian mixture model fit to the change in time spent in the quadrant housing the magnet between pre- and post-training periods was used to classify individual fish as learners or non-learners (Figure S1C). We concluded that 61% of the fish tested (total of 41) learned to avoid the robot after training (Figure S1C). Other aspects of behavior, such as swim bout frequency and average speed, remained largely unchanged (Figures S1D and S1E), showing that fish were still active and moving normally after training (Video S1). Thus, larval zebrafish rapidly learn to avoid the robot, even after it stops moving, following brief predation-like interactions.

We next characterized the time course of the avoidance. During the 30 min post-training, avoidance was relatively constant, with short-lived periods where the fish would briefly venture into the robot quadrant (Figure 1E). In a separate subset of experiments, we asked how long the avoidance would persist by removing the robot and reintroducing it once an hour post-training. We found that ~3/4 of fish continued avoiding the robot after 1 h post-training and that by 2 h, most fish (62%) stopped avoiding it (Figure S1H). Thus, CRA represents rapidly induced and relatively long-lasting avoidance behavior persisting for about 1 h after training.

The above analysis was conducted on fish screened for active exploration of the behavioral arena pre-training (see pre-training quadrant occupancy distributions and STAR Methods). However, a subset of fish did not swim evenly throughout the arena, showing a weak avoidance toward the magnet quadrant (Figure S1I). The innate tendency in this subset suggests an object avoidance neuro-behavioral program that may be co-opted during the learned avoidance seen in CRA.[49,50] It also raises the question of whether CRA reflects genuine learning or a simpler stress-induced "ON-switch" of an existing behavioral pattern. To control for this, we introduced a second assay in which the robot never moved and where the training period was replaced by 3 min of shaking in a Petri dish. Larvae manipulated in this manner did not show avoidance toward the robot post-shaking (Figure S1J), suggesting CRA is not a simple stress response in which fish avoid any object in their environment. However, the possibility still existed that CRA is a more specific switch to innate object avoidance. In that case, after such a switch, the fish should avoid all robots indiscriminately, which we tested next.

Larvae learn to distinguish benign from previously aggressive robots

To confirm that CRA induces avoidance specific to a previously aggressive robot, we modified the assay to include an additional,

(C) Brief training periods lead to prolonged avoidance behaviors. Top: schematic of experimental paradigm. Robot remains immobile in quadrant 1 (q1) during 10-min pre-training period and in q2 during 10-min post-training period. Middle/bottom row: density maps showing occupancy with trajectories overlaid for two example fish over entire pre/post-training period. Middle column: 10-s clips from training that show fish trajectories and robot positions during sample chase sequence. See also Videos S1 and S2 and Figure S2.

(D) CRA learning across fish quantified by time spent in each quadrant of the arena, averaged over 10-min pre-training (left) and post-training (right) periods ($n = 41$; $p = 0.0025$, robot quadrant pre vs. robot quadrant post, Wilcoxon test), and kernel density estimates of pre- and post-training occupancies for magnet quadrant (q1 pre and q2 post, red) and remaining three quadrants (gray). After training, fish spend less time near the robot, reflected by the area marked "#" in the histogram. 61% of fish learn (see Figure S1C; chance learner fraction would be 0%).

(E) Avoidance behavior lasts tens of minutes. Occupancy of robot housing quadrant (q1 in pre, q2 in post) shown as average over sliding window of 4 min (10-s bins). Plotted are the median and standard error of the mean (SEM) (envelopes) across five fish. Dashed line: chance quadrant occupancy level, 25%. Purple bar: periods where post-training averages are significantly below chance occupancy (significance $p < 0.05$ using a rank-sum test).

(F) Larvae learn to distinguish between aggressive and benign robots. Schematic of experiment (top) and heatmaps/trajectories. Aggressive robot (shown in red) chases fish during training; benign robot (shown blue) remains stationary in q3 throughout experiment. For half of the fish, the blue robot was the aggressor and the red was benign. See also Figure S1B.

(G) Correct identification and avoidance of aggressive robot ($n = 12$; $p = 0.0034$, magenta-pre vs. magenta-post; $p = 0.0005$, magenta-post vs. green-post; Wilcoxon test), and kernel density estimates of pre- and post-training quadrant occupancy post-training for aggressive-robot quadrant (q1 pre and q2 post, magenta) or benign-robot quadrant (q3, green) (*$p < 0.05$, **$p < 0.01$, ***$p < 0.001$). (Magenta/green is used for clarity because red/blue is swapped for 50% of experiments, see F.) After training, fish spend less time near the aggressive robot, reflected by the area marked "#" in the histogram, but they do not avoid the benign robot. See also Figures S1F and S1G.

(H) Selective avoidance of aggressive robot quantified by change in distance to each robot between post- and pre-training periods (left). Scatterplot shows increased distance kept specifically from aggressive robot, no increased distance to benign robot (right) ($n = 12$; $p = 0.0004$ (magenta, aggressive); $p = 0.35$ (green, benign); one-sample t test).

See also Figure S2. All error bars are standard error of the mean (SEM).

Please cite this article in press as: Zocchi et al., Days-old zebrafish rapidly learn to recognize threatening agents through noradrenergic and forebrain circuits, Current Biology (2024), https://doi.org/10.1016/j.cub.2024.11.057

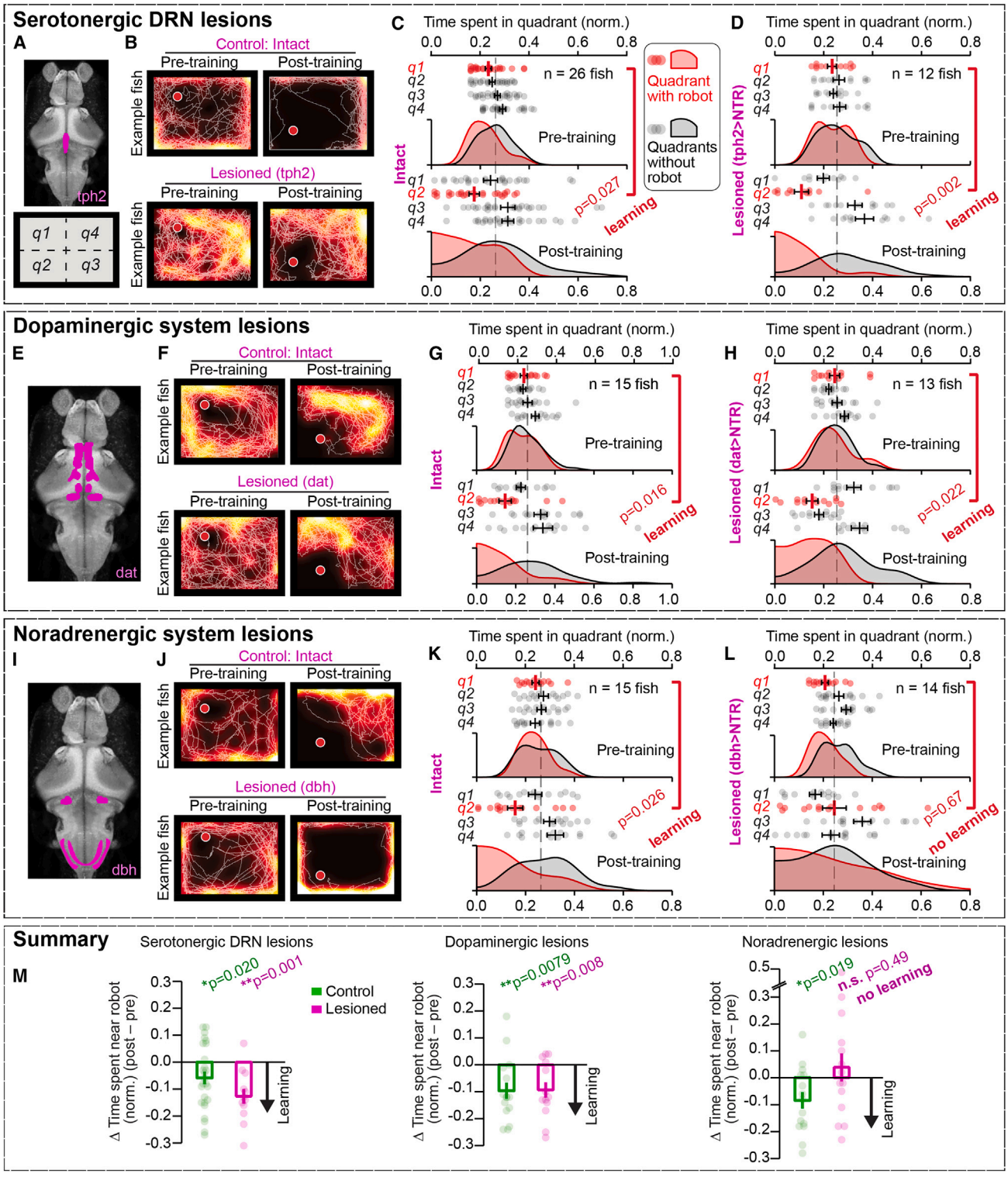

Figure 2. The noradrenergic system is required for conditioned robot avoidance learning

(A) Top: diagram showing location of tryptophan hydroxylase 2 (tph2) positive DRN neurons. Bottom: schematic of quadrant numbering. See also Figure S3A.

(B) CRA learning is intact in DRN-lesioned fish, two example fish. Density maps and trajectories of pre- and post-training behavior from an intact control (top row) and experimental (bottom row) fish.

(C) Control population data: intact fish. Scatterplot: learning across control fish quantified by quadrant occupancy, averaged over the 10-min periods (n = 26). Densities: kernel density estimates of pre- and post-training occupancy distribution of magnet quadrant (q1 pre, q2 post, red) and the remaining three quadrants

(legend continued on next page)

benign robot, identical in shape to the moving robot but always stationary and painted in a different color (Figure 1F; the aggressive robot was red for half the fish tested and blue for the other half). The other, aggressive, robot also sat immobile during the pre-training and post-training periods, but it chased the fish during training (Figure S1B). We found that fish learned to selectively avoid the aggressive robot after training, reflected in their avoidance of the quadrant with the aggressive robot but not the quadrant with the benign robot (Figures 1F and 1G), as well as an increased average distance between the fish and the aggressive robot but not the benign robot (Figure 1H). Swim frequency and swim speed remained unchanged between pre- and post-training periods (Figures S1F and S1G). These observations rule out the possibility that fish indiscriminately avoid objects in their environment due to stress-like states induced by attacks, instead showing the avoidance behavior is bound to specific identifying features of the robot. We conclude that short experiences of attack induce long-lived avoidance that is specific to previously aggressive agents in the environment.

Very young zebrafish perform CRA learning

We first observed CRA in a 2.5 × 2.0 cm^2 arena in 9–13 dpf zebrafish, as discussed above. Young (5–6 dpf) zebrafish did not show CRA in this small arena, presumably because of interference by confinement stress.[51] To test if young zebrafish perform CRA learning in a larger and therefore more naturalistic arena with less confinement stress, we created a second setup using a 6.0 cm-diameter circular arena (Figure S2A, area of circular arena is 5.65× larger). In this arena, 5–7 dpf zebrafish robustly learned CRA (Figures S2B–S2D; Video S2) after 45 s of chase (90 s total of which 45 s was chase time), showing that CRA is present from very young ages, already at 5 dpf (Figure S2E). Thus, larvae readily and robustly perform CRA learning just 1 day after they begin to swim.

The NE system is necessary for CRA learning, but the dopaminergic and serotonergic systems are not

We sought to elucidate the neural mechanisms underlying CRA. The dopaminergic, serotonergic, and NE systems have all been implicated in different forms of learning,[52–57] with roles in promoting plasticity.[56,58,59] To determine the necessity of these neuromodulatory systems in CRA, we chemogenetically lesioned each of them one by one, in fish aged 9–13 dpf, using cell-type-specific expression of nitroreductase, which causes toxin-induced cell death after incubation with the prodrug metronidazole[60] (Figures S3A–S3C). Dorsal raphe nucleus (DRN)-lesioned fish were still able to learn CRA to the level of intact controls (Figures 2A–2D, using *Tg(tph2:gal4Gal4; UAS-E1B:NTR-mCherry)* fish[61]). Similarly, fish with dopaminergic ablations were able to learn CRA (Figures 2E–2H, *Tg(dat:gal4Gal4; UAS-E1B:NTR-mCherry)* fish[62]). In contrast, NE system ablations (*Tg(dbh:gal4Gal4; UAS-E1B:NTR-mCherry)*) led to a complete loss in learning ability (Figures 2I–2L; all summarized in Figure 2M). Similar numbers of fish avoided the non-robot quadrants and the robot quadrant, indicating an inability to correctly associate the robot with danger (Figures 2L and 2M). Some NE-system ablated fish showed increased thigmotactic behavior[63]; however, this was not consistent across all fish tested (Figures S3G–S3I). Other aspects of swim behavior, like swim frequency and speed, remained similar between pre- and post-training periods and between lesioned and control conditions for all neuromodulatory ablations (Figures S4A–S4F). Thus, the NE system, specifically, and not the dopaminergic or serotonergic systems, is required for larval zebrafish to perform CRA learning.

LC neuron responses during CRA are consistent with learning signals

Building on the identification of the NE system, which includes the LC as a driver for learning, we turned our attention to neural activity patterns associated with the training. We used a reduced preparation that captured the core components of CRA training in which a head-fixed, agar-embedded zebrafish experiences the approach of the robot, its close presence during a "sit" period, and its retreat (Figures 3A and 3B). We first confirmed that this basic restrained paradigm could elicit learning: agar-embedded fish that experienced the approaching robot and were subsequently freed showed avoidance of the robot (Figure S5A). Next, using swept confocally aligned planar excitation (SCAPE) microscopy[64,65] (Figures 3A and S5B), we imaged LC activity in *Tg(dbh:Gal4; UAS:GCaMP6f)* fish aged 9–13 dpf. This population showed strong responses

(gray). Dashed line shows chance occupancy (25%). Controls expressed either *Tg(tph2:Gal4)* or *Tg(UAS-E1B:NTR-mCherry)* and were incubated in metronidazole prior to experiment.

(D) CRA learning is intact in DRN-lesioned fish, population data (n = 12 fish). *Tg(tph2:Gal4; UAS-E1B:NTR-mCherry)* fish were previously incubated in metronidazole.

(E) Schematic of dopamine transporter (dat) expression for dopaminergic ablations. See also Figure S3B.

(F) Dopaminergic ablations do not impair CRA learning, example control and lesioned fish.

(G and H) Dopaminergic ablations do not impair learning; population data represented as in (C) and (D). Controls (n = 15) were *Tg(dat:Gal4)* or *Tg(UAS-E1B:NTR-mCherry)*, lesioned fish were *Tg(dat:Gal4; UAS-E1B:NTR-mCherry)* fish (n = 13), both previously incubated in metronidazole.

(I) Schematic of dopamine beta-hydroxylase (dbh) expression for noradrenergic system ablations. See also Figure S3C.

(J) Noradrenergic ablation eliminates CRA learning in an example fish.

(K and L) Noradrenergic ablations eliminate learning, population data. Controls (n = 15) were *Tg(dbh:Gal4)* or *Tg(UAS-E1B:NTR-mCherry)*, lesioned fish (n = 14) were *Tg(dbh:Gal4; UAS-E1B:NTR-mCherry)*, both previously incubated in metronidazole. Scatterplot statistics are between the magnet quadrant pre-training (q1) and post-training (q2) using the Wilcoxon test.

(M) Summaries of ablation behavioral experiments. Plotted are differences in occupancies of magnet-housing quadrants pre- and post-training (q2 post – q1 pre). CRA is manifested as a downward trend of the average (black arrows). Magenta data are from lesioned conditions; green is intact control. Statistics reflect one-sample t tests, testing deviance from a population mean of 0. Serotonergic and dopaminergic system ablations do not impair learning; noradrenergic system ablation abolishes learning.

See also Figure S4.

Statistical tests for C, D, G, H, K, and L were Wilcoxon tests. All error bars reflect SEMs.

Please cite this article in press as: Zocchi et al., Days-old zebrafish rapidly learn to recognize threatening agents through noradrenergic and forebrain circuits, Current Biology (2024), https://doi.org/10.1016/j.cub.2024.11.057

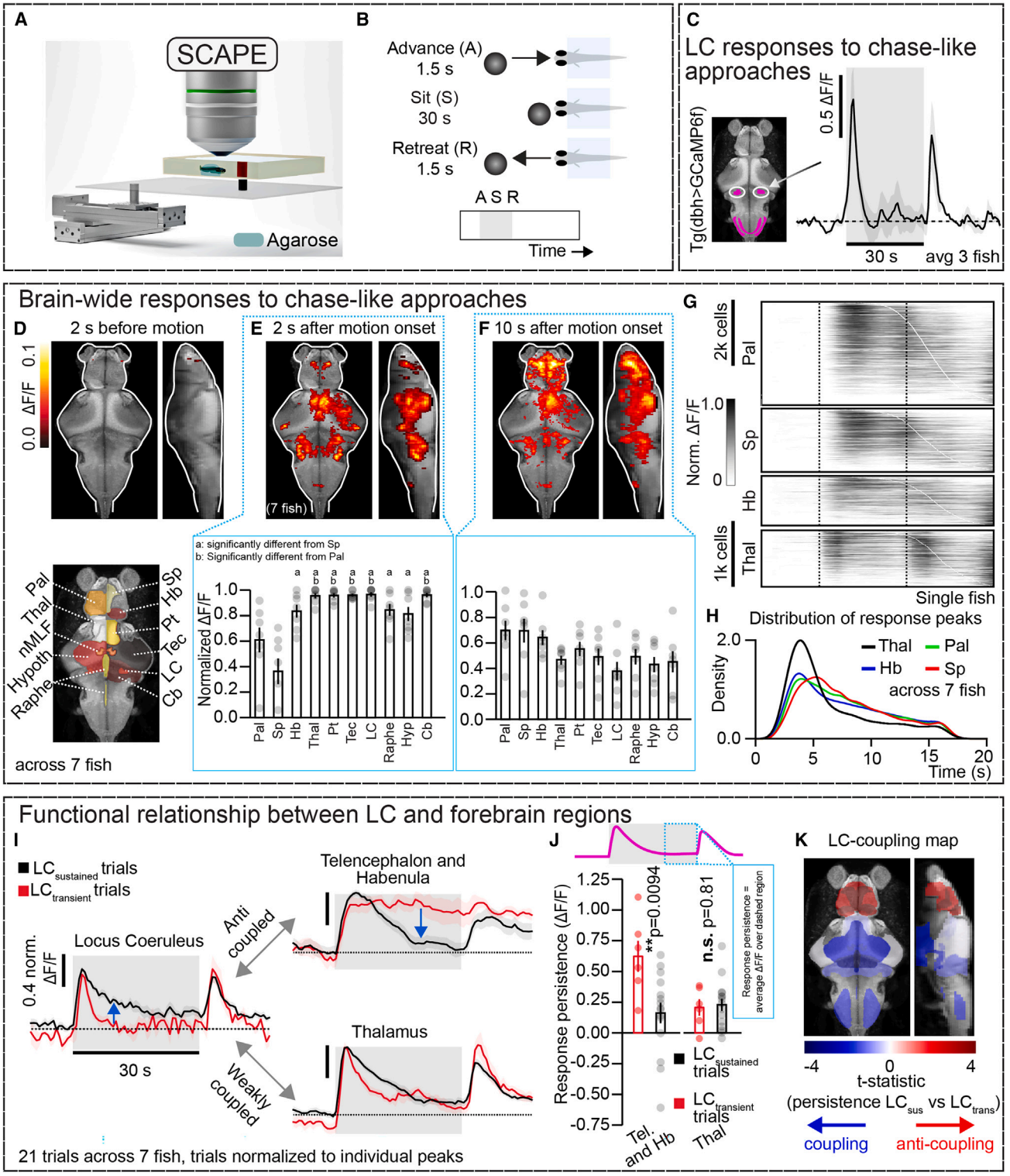

Figure 3. Whole-brain imaging of chase-like robot approaches reveal coupled responses in LC and across the forebrain

(A) Schematic of experimental setup. Agarose-embedded *Tg(dbh:Gal4; UAS:GCaMP6f)* or *Tg(elavl3:H2B-GCaMP7f)* fish were exposed to moving robot and imaged with a SCAPE microscope. See also Figures S5A and S5B.

(B) Schematic of stimulus paradigm. Chase-like approaches consisted of straight robot motion toward the fish, robot was slightly offset toward the left. Motion lasted 1.5 s, followed by a 30-s sit period, followed by retreat to its original position.

(legend continued on next page)

Please cite this article in press as: Zocchi et al., Days-old zebrafish rapidly learn to recognize threatening agents through noradrenergic and forebrain circuits, Current Biology (2024), https://doi.org/10.1016/j.cub.2024.11.057

that were time locked to robot motion, lasting about 7 s, and were strongest during robot approach and retreat (Figure 3C). Interestingly, LC responses were much reduced when the robot moved side to side (Figure S5C), a stimulus that did not elicit avoidance in free swimming fish (Figure S5D). Altogether, these experiments are consistent with a learning algorithm in which robot motion, especially attack-like movements in the approach period, serve as the learning signal,[66] analogous to an unconditioned stimulus (US) in the framework of classical conditioning.

Whole-brain light-sheet imaging reveals LC-coupled populations encoding the robot experience

In search of the neural implementation of CRA, we asked how the entire brain responds to robot approach and close presence and how such responses relate to the LC responses described above. We imaged larval zebrafish, aged 9–13 dpf, with a genetically encoded calcium sensor expressed in most neurons (*Tg(elavl3:GCaMP7f)*, Figure S5B). We observed responses during the approach relative to baseline (Figure 3D) in multiple regions (Figure 3E), which we identified through registration to an anatomy atlas[67] as including the LC, pallium, subpallium, habenula, thalamus, pretectum, tectum, serotonergic raphe, hypothalamus, and cerebellum (Figure 3E).

We reasoned that the brain may contain a representation of the robot presence, independent of its motion, analogous to a conditioned stimulus (CS) that, through training, gets bound to evasive actions. We therefore searched for such representations by looking for populations showing elevated activity during the sit portion of the stimulus. Most of the regions active during the approach showed decaying activity during the sit period (Figure 3F). However, the pallium and subpallium were unique in showing persistently elevated activity during the sit period (Figures 3E, 3F, and S5E). Indeed, these regions, together with the habenula, also contained significantly more neurons, with activity peaking later in the robot stimulus—during the sit portion—than other regions of the forebrain like the thalamus (Figures 3G and 3H). Thus, our whole-brain imaging results suggested that brain activity encoding close robot presence is found across the telencephalon and habenula.

Since the NE system is necessary for learning, and regions of the telencephalon and habenula showed sustained responses during the robot experience, suggesting that they might encode the presence of the robot, we asked whether the LC and forebrain showed functional coupling. We noticed that on some trials, LC activity was more transient, and on other trials, it was more sustained (Figure 3I). We observed strong coupling between the LC and the telencephalon and habenula, where more transient LC responses were followed by more sustained responses in these latter regions, and more sustained LC responses were followed by more transient responses (Figures 3I, 3J, and S5F). No other areas analyzed showed this functional relationship to the LC (Figures 3I–3K). For comparison, repeating the analysis using the thalamus instead of LC did not yield a similar inverse relationship with the telencephalon and habenula (Figure S5G). Finally, there was no functional coupling between the telencephalon and habenula and the NE cluster of the medulla oblongata (NE-MO[68]) (Figure S5H). Therefore, the relationship was specific to the LC. The strong coupling between LC and telencephalon/habenula responses, in combination with the observation that the LC is necessary for CRA learning, led us to consider the hypothesis that the telencephalon and habenula are necessary components of the learning mechanism.

Forebrain regions are necessary for CRA

To test whether the telencephalon and habenula are necessary for CRA learning, we vacuum aspirated a large fraction of these regions in fish aged 9–13 dpf (Figures 4A and S3D) and, following recovery, tested the fish's learning ability. Lesioned fish still swam and explored (Figures S3J, S4G, and S4H) but were not able to learn CRA (Figures 4B–4D). Thus, consistent with the measured responses (Figures 3E and 3F) and functional coupling to the LC (Figures 3I and 3J), the combination of the telencephalon and the habenula are necessary for CRA learning. Next, we specifically lesioned the habenula using two-photon cell-resolution ablation. To control for nonspecific effects of the laser and

(C) Average activity in LC in *Tg(dbh:Gal4; UAS:GCaMP6f)* fish shows responses to robot motion (approach and retreat; strongest during approach). Envelope reflects SEM. See also Figures S5C and S5D.

(D–F) Whole-brain responses to stimulus averaged over three trials across seven fish. Z-Brain atlas-identified brain regions are displayed on a reference brain (D, bottom). Threshold heatmaps (see STAR Methods) showing maximum intensity projections of ΔF/F responses across voxels, 2 s prior to motion onset (D, top), 2 s following onset (E, top), and 10 s after onset (F, top). Normalized ΔF/F in regions across larval brain over 21 trials in 7 fish (bottom bar plots in E and F). Each point represents ΔF/F averaged over neurons in the given region for a single trial, normalized to their peak values across trials. Telencephalon showed stronger sustained responses (left) than most other regions (right). Bars sharing letters are statistically different from subpallium (a) and pallium (b) (ANOVA followed by Tukey's honestly significant difference test). Pal, pallium; Sp, subpallium; Hb, habenula; Thal, thalamus; Pt, pretectum; Tec, optic tectum; LC, locus coeruleus; Raphe, dorsal raphe nucleus; Hyp, hypothalamus; Cb, cerebellum. Error bars reflect SEMs. See also Figure S5E.

(G) Rasters showing single-cell ΔF/F across regions of the telencephalon and in the habenula across six fish. Responses normalized to their peak values and sorted by centroid, $\Sigma_t t(\Delta F/F)(t)/\Sigma_t(\Delta F/F)(t)$. White ticks indicate trace centroid.

(H) Kernel density estimates of distributions of time to peak across single cells in different regions of the forebrain across 21 trials in 7 fish. Telencephalon and habenula have more cells peaking later in the stimulus than thalamus ($p < 0.0001$ for Hb to Thal, Pal to Thal, and Sp to Thal, Kolmogorov-Smirnov test [K-S test]).

(I) Responses in telencephalon and habenula are functionally coupled to LC responses. Responses on single trials, averaged across neurons of the LC; thalamus; and combined pallium, subpallium, and habenula (telencephalon and habenula); with trials grouped according to whether the cell-averaged LC response was sustained (black) or transient (red) (see STAR Methods). Transience of the LC response was predictive of how sustained the telencephalic and habenular responses were (transient LC response was associated with sustained telencephalon and habenula response; arrows); and less so for thalamus. 21 trials in 7 fish. Line: average, envelope: SEM. Each trial's response was normalized to its peak. See (J) for statistical test. See also Figures S5F–S5H.

(J) Response persistence (as defined in inset) in telencephalon/habenula and thalamus on trials with transient (red) vs. sustained (black) LC responses. Statistics were independent t tests for differences between transient LC (red) and sustained LC (black) groups. Error bars reflect SEM.

(K) Response persistence (as in J) across different brain regions. Plotted over a representative brain (gray) are the t statistics (from independent t tests) between trials with transient vs. trials with sustained LC responses for different regions.

Please cite this article in press as: Zocchi et al., Days-old zebrafish rapidly learn to recognize threatening agents through noradrenergic and forebrain circuits, Current Biology (2024), https://doi.org/10.1016/j.cub.2024.11.057

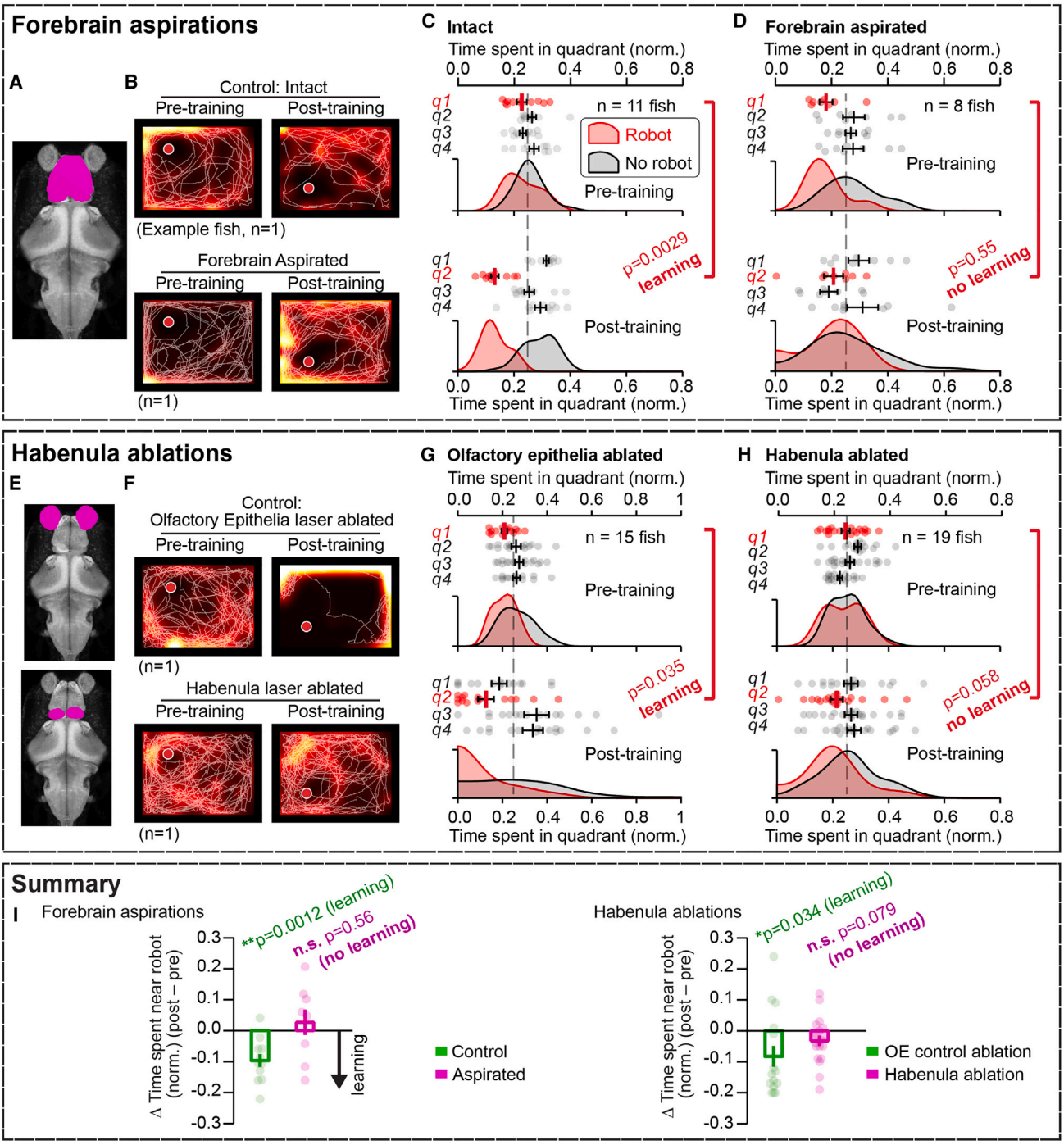

Figure 4. The forebrain and the habenula, specifically, are required for learned avoidance

(A) Diagram showing extent of vacuum aspirations of forebrain. See also Figure S3D.

(B) Heatmaps with trajectories show pre- and post-training behavior from one intact control (top row) and one aspirated experimental fish (bottom row). Note, forebrain-aspirated example fish shows no learned avoidance post-training.

(C) Control fish ($n = 11$) avoid robot after training. Scatterplot: learning across control fish quantified by quadrant occupancy (time spent in quadrants), averaged over experiment periods. Densities: kernel density estimates for pre- and post-training occupancy distributions in robot quadrant (q1 pre and q2 post, red), or remaining three quadrants (gray). Dashed line represents chance occupancy (25%). Statistics for all scatterplots are between the magnet quadrant pre-training (q1) and post-training (q2) using the Wilcoxon test.

(D) Forebrain-aspirated fish do not learn. Ablated fish ($n = 8$) had their forebrains vacuum aspirated. Control data were combined from two groups: siblings of the aspirated fish; or fish from a different clutch who were anesthetized and embedded like the ablated group, but who did not undergo ablation.

(E) Schematic for two-photon laser ablations of habenula (bottom row) and, as a control, olfactory epithelia (OE) (top row). See also Figures S3E and S3F.

(legend continued on next page)

Please cite this article in press as: Zocchi et al., Days-old zebrafish rapidly learn to recognize threatening agents through noradrenergic and forebrain circuits, Current Biology (2024), https://doi.org/10.1016/j.cub.2024.11.057

cell death, we ablated the olfactory epithelium for comparison (Figures 4E, S3E, and S3F), which did not impair learning (Figures 4F and 4G). Habenula ablations led to a near-complete loss of learning (Figures 4F and 4H). Thus, the habenula is necessary for CRA learning. Other aspects of swim behavior were unchanged (Figures S3K, S4I, and S4J). In sum, the telencephalon and habenula are necessary for CRA, consistent with the role of forebrain circuits in higher-order cognitive functions.[18,69,70] The habenula, specifically, is necessary, consistent with its proposed role of linking limbic circuits of the forebrain and regions of the mid- and hindbrain.[71–73]

Taking together our behavioral, ablation, and imaging results, we demonstrate rapidly learned recognition of aggressive agents in a nascent vertebrate nervous system. This associative learning relies on a multiregional network, including NE signaling, with LC activity consistent with a learning signal encoding the movement of the attacker, as well as populations distributed across the forebrain, particularly the habenula, whose activity represents the presence of the object, which gets associated with danger through experience.

DISCUSSION

Fast, specific predator recognition learning in a nascent vertebrate nervous system

Here, we have demonstrated that predator learning emerges early in the development of a vertebrate brain, on the day that the fish start to swim with reliable coordination and to hunt for food—5 dpf—and prior to when they reliably perform social behaviors like shoaling.[74] While neonates are constantly learning to interface with their environments, for example, through motor development,[75,76] learning what to eat,[13,77–79] or how to communicate,[80] most of these learned behaviors develop over relatively long periods of time, sometimes with the help of their parents.[79,81,82] Predator avoidance learning, on the other hand, is self-taught and must be rapid since every predator-prey encounter has the potential to turn lethal.[83] The task is further complicated by having to identify cues most relevant for future predator recognition in the midst of the barrage of sensory input produced by a predatory attack. Indeed, CRA drives rapidly induced learning, resulting in a memory lasting over an hour. This duration could be beneficial in nature as the greatest risk of attack by an individual predator following an initial predatory attempt is in the period immediately following. As time moves on, the need to remember the identity of a specific predator decreases due to factors like the animals physically separating and the predator targeting a different prey individual. Other factors like enhanced memory following multiple encounters, memory retention improving with age beyond the larval and into the juvenile and adult stages, or learning being more efficient with the use of more realistic predatory robots or real predators are worth following up on with future studies. Moreover, larvae are able to identify and selectively avoid the correct robot in two-robot conditioning experiments, showing an ability to extract identifying features without over-generalizing. This is in contrast to most forms of predator learning studied on longer training timescales or in older animals that usually rely on associating olfactory cues—such as alarm substances secreted by conspecifics—with the predator, a process one step removed from an actual predatory attack.[83–85] Furthermore, larval brain volumes contain around 100 times fewer neurons than adults, and neuron number is believed to correlate to cognitive ability in animals.[86–88] Our behavioral assay has thus uncovered the ability of a compact brain to extract key identifying features of dangerous agents in their environments and to use them to drive future behavioral interactions. Similar to social behaviors between conspecifics,[4,89] predator avoidance is a task that young larvae must necessarily deal with in the natural environment[90]; and brains are adapted to solving ethologically relevant tasks, a theme exploited in some of the most efficient learning assays.[91–93] Indeed, a fraction of naive fish showed a weak avoidance for the robot pre-training (Figure S1I), hinting at existing neural pathways for innate (non-learned) avoidance toward novel entities in the environment.[94,95] It is possible that the early emergence of CRA during development is facilitated by extending these pathways, for instance, by learning to bind them to specific identifying features of threatening agents as suggested by the two-robot experiments (Figures 1F–1H). In sum, we have identified predator learning as one of the earliest, most rapid forms of learning in a nascent vertebrate brain.

Neural mechanisms underlying rapid predator recognition learning

Brain-wide calcium imaging identified the LC and forebrain populations across the telencephalon and habenula[17,18,26,73]—a diencephalic structure that also forms part of the forebrain[47,48]—as likely candidates mediating the learning seen in CRA. The imaging results are consistent with a mechanism involving a learning signal in the form of NE[96,97] signaling onto pallial, subpallial, and habenular[17,98–100] circuits.[101] Regions of the larval pallium and subpallium have been linked via anatomical, genetic, and ablation studies to homologous mammalian regions like the amygdala, hippocampus, and basal ganglia.[102–104] A large body of work implicates mammalian limbic regions in emotionally driven learning like fear conditioning.[53,105,106] Electrophysiological, pharmacological, and lesion studies have produced a picture where NE signaling of unconditioned stimuli[107,108] onto amygdalar circuits leads to potentiation of sensory

(F) Habenula-ablated fish does not learn (bottom) but control olfactory-epithelium-ablated fish does (top), example animals. Note lack of avoidance post-training in habenula-ablated fish.
(G) Olfactory-epithelium-ablated control fish learn, population data (n = 15 fish, two-photon ablation).
(H) Habenula-ablated fish do not learn, population data (n = 19 fish, two-photon ablation).
(I) Summaries of ablation behavioral experiments showing necessity of forebrain and habenula for CRA learning. Plotted are differences in occupancies of magnet-housing quadrants pre- and post-training (q2 post – q1 pre) across different ablations. CRA is manifested as a downward value of the average (black arrows). Magenta data are from ablated conditions, green is from controls. Statistics for scatterplots reflect one-sample t tests, testing deviance from a population mean of 0.
See also Figure S4. All error bars reflect SEM.

responses to conditioned stimuli across limbic regions.[57,109] Our imaging and behavioral findings, together, suggest that similar mechanisms may operate during larval CRA learning.

Coupling between LC and telencephalic/habenular response dynamics

We describe a relationship between dynamics in the LC and in the telencephalon/habenula, where transient responses in the former region are correlated to persistent activity in the latter ones. While norepinephrine has complex effects on neural circuit function,[110] it is believed that α_1 and β-adrenergic receptors[111,112] often have opposing effects on neural circuits. The functional relationship we describe could arise from an interplay between the excitatory and potentially delayed inhibitory effects of NE signaling on different receptor types, whereby transient LC responses preferentially drive excitatory effects in pallial, subpallial and habenular circuits, while longer LC responses allow inhibitory effects to manifest. Future studies could address this mechanism, starting by imaging norepinephrine dynamics in these forebrain populations, as well as its function for learning.

Our behavioral experiments also uncovered a necessary role for the habenula in CRA. However, it is important to note that the habenula is a complex, heterogeneous structure made up of subcircuits with different presumed functions and distinct projection patterns.[17,72,98–100,113] Future work will be required to dissect out the precise subregions within the habenula involved in CRA. Finally, a general relationship—of course, with exceptions—is believed to exist between cognitive ability and number of neurons across brain regions.[86–88] It is therefore remarkable that a small developing vertebrate brain of $\sim 10^5$ neurons—$\sim$1/500th the number in a mouse brain—is capable of rapidly learning characteristics of agents in the environment within minute-long experiences. This contrasts with the state of the art in artificial learning systems which, although capable of significantly more complex tasks, nevertheless require orders of magnitude more computing elements and training data to do so. How biological brains perform so efficiently is a key open question for neuroscience,[50] likely having to do with the distribution of learning tasks across a highly modular nervous system, as well as the wide broadcasting of learning signals consistent with the NE LC signal observed here. The study of whole-brain signals during survival-critical, rapid learning in a small brain may therefore yield insights into the design of artificial systems, as well as help unravel the relationship between evolutionarily hard-wired behaviors and adaptable learned ones.

RESOURCE AVAILABILITY

Lead contact

Further information and requests for resources and reagents should be directed to and will be fulfilled by the lead contact, Misha Ahrens (ahrensm@janelia.hhmi.org).

Materials availability

Tg(dbh:Gal4) was generated for this study using recombination of Gal4FF into bacterial artificial chromosome (BAC)[113,114] CH211-270H11, followed by Tol2 transgenesis (available upon request and will be deposited to the Zebrafish International Resource Center [ZIRC]).[115]

Data and code availability

- All behavioral datasets and an example imaging dataset have been deposited at Mendeley Data and are publicly available as of the date of publication at Mendeley Data: http://www.doi.org/10.17632/wkxwggvfbx.1.
- All original code has been deposited at Mendeley Data and is publicly available at Mendeley Data: http://www.doi.org/10.17632/wkxwggvfbx.1.
- Any additional information required to reanalyze the data reported in this paper is available from the lead contact upon request.

ACKNOWLEDGMENTS

We thank Yu Mu, Brett Mensh, Joshua Dudman, Florian Engert, Rob Johnson, Shriya Pai, Weiyu Chen, Jing Xuan Lim, Ann Hermundstad, Andrew Bolton, and Ahrens lab members for their feedback on the manuscript. We are grateful to Vivek Jayaraman and Ann Hermundstad for the discussions. We thank Citlali Perez Campos, Wenze Li, and Venkatakaushik Voleti for their assistance with SCAPE microscopy. We thank the Janelia Vivarium, Janelia Experimental Technology, and Project Technical Resources and Gudrun Ihrke for their support. This research was supported in part by the Howard Hughes Medical Institute (M.B.A.). Additional funding was received as follows: M.B.A., a Simons Foundation Collaboration on Global Brain award; E.M.C.H., a Simons Foundation Collaboration on Global Brain award, NIH U01, and NIH UF1; and D.A.P., NIH R35 and NIH UF1.

AUTHOR CONTRIBUTIONS

D.Z. conceived of the project, developed the methodology, conducted experiments, and wrote the paper. M.B.A. conceived of the project, developed the methodology, administered and supervised the project, and wrote the paper. E.M.-L., C.S., D.A.P., and E.M.C.H. developed the methodology. M.N. conducted experiments. I.S. developed visualizations.

DECLARATION OF INTERESTS

The authors declare no competing interests.

STAR★METHODS

Detailed methods are provided in the online version of this paper and include the following:

- KEY RESOURCES TABLE
- EXPERIMENTAL MODEL DETAILS
  - Fish
- METHOD DETAILS
  - Behavior – Setup
  - Behavior - Analysis and Tracking
  - Behavior - Assays
  - Ablations
  - Imaging - Setup and Robot Stimuli
  - Imaging - Processing and Analysis
- QUANTIFICATION AND STATISTICAL ANALYSIS

SUPPLEMENTAL INFORMATION

Supplemental information can be found online at https://doi.org/10.1016/j.cub.2024.11.057.

Received: July 12, 2024
Revised: October 3, 2024
Accepted: November 22, 2024
Published: December 23, 2024

REFERENCES

1. Kappel, J.M., Förster, D., Slangewal, K., Shainer, I., Svara, F., Donovan, J.C., Sherman, S., Januszewski, M., Baier, H., and Larsch, J. (2022).

Visual recognition of social signals by a tectothalamic neural circuit. Nature *608*, 146–152.

2. Breed, M.D., Leger, E.A., Pearce, A.N., and Wang, Y.J. (1998). Comb wax effects on the ontogeny of honey bee nestmate recognition. Anim. Behav. *55*, 13–20. https://doi.org/10.1006/anbe.1997.0581.
3. Wei, D., Talwar, V., and Lin, D. (2021). Neural circuits of social behaviors: innate yet flexible. Neuron *109*, 1600–1620. https://doi.org/10.1016/j.neuron.2021.02.012.
4. Larsch, J., and Baier, H. (2018). Biological motion as an innate perceptual mechanism driving social affiliation. Curr. Biol. *28*, 3523–3532.e4. https://doi.org/10.1016/j.cub.2018.09.014.
5. Anneser, L., Alcantara, I.C., Gemmer, A., Mirkes, K., Ryu, S., and Schuman, E.M. (2020). The neuropeptide Pth2 dynamically senses others via mechanosensation. Nature *588*, 653–657. https://doi.org/10.1038/s41586-020-2988-z.
6. Sih, I., Ziemba, I., and Harding, K.C. (2000). New insights on how temporal variation in predation risk shapes prey behavior. Trends Ecol. Evol. *15*, 3–4. https://doi.org/10.1016/S0169-5347(99)01766-8.
7. Griffin, A.S., Evans, C.S., and Blumstein, D.T. (2001). Learning specificity in acquired predator recognition. Anim. Behav. *62*, 577–589. https://doi.org/10.1006/anbe.2001.1781.
8. Ferrari, M.C.O., Gonzalo, A., Messier, F., and Chivers, D.P. (2007). Generalization of learned predator recognition: an experimental test and framework for future studies. Proc. Biol. Sci. *274*, 1853–1859. https://doi.org/10.1098/rspb.2007.0297.
9. Friedrich, R.W., Genoud, C., and Wanner, A.A. (2013). Analyzing the structure and function of neuronal circuits in zebrafish. Front. Neural Circuits *7*, 71. https://doi.org/10.3389/fncir.2013.00071.
10. Hill, A., Howard, C.V., Strahle, U., and Cossins, A. (2003). Neurodevelopmental defects in zebrafish (Danio rerio) at environmentally relevant dioxin (TCDD) concentrations. Toxicol. Sci. *76*, 392–399. https://doi.org/10.1093/toxsci/kfg241.
11. Hinsch, K., and Zupanc, G.K.H. (2007). Generation and long-term persistence of new neurons in the adult zebrafish brain: A quantitative analysis. Neuroscience *146*, 679–696. https://doi.org/10.1016/j.neuroscience.2007.01.071.
12. Valente, A., Huang, K.-H., Portugues, R., and Engert, F. (2012). Ontogeny of classical and operant learning behaviors in zebrafish. Learn. Mem. *19*, 170–177. https://doi.org/10.1101/lm.025668.112.
13. Oldfield, C.S., Grossrubatscher, I., Chávez, M., Hoagland, A., Huth, A.R., Carroll, E.C., Prendergast, A., Qu, T., Gallant, J.L., Wyart, C., et al. (2020). Experience, circuit dynamics, and forebrain recruitment in larval zebrafish prey capture. eLife *9*, e56619. https://doi.org/10.7554/eLife.56619.
14. Hunt, P.S., Fanselow, M.S., Richardson, R., Mauk, M.D., Freeman, J.H., Jr., and Stanton, M.E. (2007). Synapses, circuits, and the ontogeny of learning. Dev. Psychobiol. *49*, 649–663. https://doi.org/10.1002/dev.20250.
15. Aizenberg, M., and Schuman, E.M. (2011). Cerebellar-dependent learning in larval zebrafish. J. Neurosci. *31*, 8708–8712. https://doi.org/10.1523/JNEUROSCI.6565-10.2011.
16. Hinz, F.I., Aizenberg, M., Tushev, G., and Schuman, E.M. (2013). Protein synthesis-dependent associative long-term memory in larval zebrafish. J. Neurosci. *33*, 15382–15387. https://doi.org/10.1523/JNEUROSCI.0560-13.2013.
17. Palumbo, F., Serneels, B., Pelgrims, R., and Yaksi, E. (2020). The zebrafish dorsolateral habenula is required for updating learned behaviors. Cell Rep. *32*, 108054. https://doi.org/10.1016/j.celrep.2020.108054.
18. Lal, P., Tanabe, H., Suster, M.L., Ailani, D., Kotani, Y., Muto, A., Itoh, M., Iwasaki, M., Wada, H., Yaksi, E., et al. (2018). Identification of a neuronal population in the telencephalon essential for fear conditioning in zebrafish. BMC Biol. *16*, 45. https://doi.org/10.1186/s12915-018-0502-y.
19. Dempsey, W.P., Du, Z., Nadtochiy, A., Smith, C.D., Czajkowski, K., Andreev, A., Robson, D.N., Li, J.M., Applebaum, S., Truong, T.V., et al. (2022). Regional synapse gain and loss accompany memory formation in larval zebrafish. Proc. Natl. Acad. Sci. USA *119*, e2107661119. https://doi.org/10.1073/pnas.2107661119.
20. Lin, Q., Manley, J., Helmreich, M., Schlumm, F., Li, J.M., Robson, D.N., Engert, F., Schier, A., Nöbauer, T., and Vaziri, A. (2020). Cerebellar neurodynamics predict decision timing and outcome on the single-trial level. Cell *180*, 536–551.e17. https://doi.org/10.1016/j.cell.2019.12.018.
21. Najac, M., McLean, D.L., and Raman, I.M. (2023). Synaptic variance and action potential firing of cerebellar output neurons during motor learning in larval zebrafish. Curr. Biol. *33*, 3299–3311.e3. https://doi.org/10.1016/j.cub.2023.06.045.
22. Harmon, T.C., Magaram, U., McLean, D.L., and Raman, I.M. (2017). Distinct responses of Purkinje neurons and roles of simple spikes during associative motor learning in larval zebrafish. eLife *6*, e22537. https://doi.org/10.7554/eLife.22537.
23. Matsuda, K., Yoshida, M., Kawakami, K., Hibi, M., and Shimizu, T. (2017). Granule cells control recovery from classical conditioned fear responses in the zebrafish cerebellum. Sci. Rep. *7*, 11865. https://doi.org/10.1038/s41598-017-10794-0.
24. Lovett-Barron, M. (2021). Learning-dependent neuronal activity across the larval zebrafish brain. Curr. Opin. Neurobiol. *67*, 42–49. https://doi.org/10.1016/j.conb.2020.07.006.
25. Groneberg, A.H., Marques, J.C., Martins, A.L., Diez Del Corral, R.D., de Polavieja, G.G., and Orger, M.B. (2020). Early-life social experience shapes social avoidance reactions in larval zebrafish. Curr. Biol. *30*, 4009–4021.e4.
26. Torigoe, M., Islam, T., Kakinuma, H., Fung, C.C.A., Isomura, T., Shimazaki, H., Aoki, T., Fukai, T., and Okamoto, H. (2021). Zebrafish capable of generating future state prediction error show improved active avoidance behavior in virtual reality. Nat. Commun. *12*, 5712. https://doi.org/10.1038/s41467-021-26010-7.
27. Lee, T.J., and Briggman, K.L. (2023). Visually guided and context-dependent spatial navigation in the translucent fish Danionella cerebrum. Curr. Biol. *33*, 5467–5477.e4. https://doi.org/10.1016/j.cub.2023.11.030.
28. Silva, A.J., Kogan, J.H., Frankland, P.W., and Kida, S. (1998). CREB and memory. Annu. Rev. Neurosci. *21*, 127–148. https://doi.org/10.1146/annurev.neuro.21.1.127.
29. Yin, J.C.P., Wallach, J.S., Del Vecchio, M., Wilder, E.L., Zhou, H., Quinn, W.G., and Tully, T. (1994). Induction of a dominant negative CREB transgene specifically blocks long-term memory in Drosophila. Cell *79*, 49–58. https://doi.org/10.1016/0092-8674(94)90399-9.
30. Alberini, C.M., Ghirardi, M., Huang, Y.Y., Nguyen, P.V., and Kandel, E.R. (1995). A molecular switch for the consolidation of long-term memory: cAMP-inducible gene expression. Ann. N. Y. Acad. Sci. *758*, 261–286. https://doi.org/10.1111/j.1749-6632.1995.tb24833.x.
31. Hwang, F.-J., Roth, R.H., Wu, Y.-W., Sun, Y., Kwon, D.K., Liu, Y., and Ding, J.B. (2022). Motor learning selectively strengthens cortical and striatal synapses of motor engram neurons. Neuron *110*, 2790–2801.e5. https://doi.org/10.1016/j.neuron.2022.06.006.
32. Yang, G., Pan, F., and Gan, W.-B. (2009). Stably maintained dendritic spines are associated with lifelong memories. Nature *462*, 920–924. https://doi.org/10.1038/nature08577.
33. Xu, T., Yu, X., Perlik, A.J., Tobin, W.F., Zweig, J.A., Tennant, K., Jones, T., and Zuo, Y. (2009). Rapid formation and selective stabilization of synapses for enduring motor memories. Nature *462*, 915–919. https://doi.org/10.1038/nature08389.
34. Yang, Y., Liu, D.Q., Huang, W., Deng, J., Sun, Y., Zuo, Y., and Poo, M.M. (2016). Selective synaptic remodeling of amygdalocortical connections associated with fear memory. Nat. Neurosci. *19*, 1348–1355. https://doi.org/10.1038/nn.4370.
35. Chau, L.S., and Galvez, R. (2012). Amygdala's involvement in facilitating associative learning-induced plasticity: a promiscuous role for the amygdala in memory acquisition. Front. Integr. Neurosci. *6*, 92. https://doi.org/10.3389/fnint.2012.00092.

36. Redondo, R.L., Kim, J., Arons, A.L., Ramirez, S., Liu, X., and Tonegawa, S. (2014). Bidirectional switch of the valence associated with a hippocampal contextual memory engram. Nature *513*, 426–430. https://doi.org/10.1038/nature13725.

37. Roy, D.S., Arons, A., Mitchell, T.I., Pignatelli, M., Ryan, T.J., and Tonegawa, S. (2016). Memory retrieval by activating engram cells in mouse models of early Alzheimer's disease. Nature *531*, 508–512. https://doi.org/10.1038/nature17172.

38. Packard, M.G., and Knowlton, B.J. (2002). Learning and memory functions of the basal ganglia. Annu. Rev. Neurosci. *25*, 563–593. https://doi.org/10.1146/annurev.neuro.25.112701.142937.

39. Roy, D.S., Park, Y.-G., Kim, M.E., Zhang, Y., Ogawa, S.K., DiNapoli, N., Gu, X., Cho, J.H., Choi, H., Kamentsky, L., et al. (2022). Brain-wide mapping reveals that engrams for a single memory are distributed across multiple brain regions. Nat. Commun. *13*, 1799. https://doi.org/10.1038/s41467-022-29384-4.

40. Wheeler, A.L., Teixeira, C.M., Wang, A.H., Xiong, X., Kovacevic, N., Lerch, J.P., McIntosh, A.R., Parkinson, J., and Frankland, P.W. (2013). Identification of a functional connectome for long-term fear memory in mice. PLoS Comput. Biol. *9*, e1002853. https://doi.org/10.1371/journal.pcbi.1002853.

41. Card, G., and Dickinson, M.H. (2008). Visually mediated motor planning in the escape response of *Drosophila*. Curr. Biol. *18*, 1300–1307. https://doi.org/10.1016/j.cub.2008.07.094.

42. Yilmaz, M., and Meister, M. (2013). Rapid innate defensive responses of mice to looming visual stimuli. Curr. Biol. *23*, 2011–2015. https://doi.org/10.1016/j.cub.2013.08.015.

43. Gabbiani, F., Krapp, H.G., Koch, C., and Laurent, G. (2002). Multiplicative computation in a visual neuron sensitive to looming. Nature *420*, 320–324. https://doi.org/10.1038/nature01190.

44. Evans, D.A., Stempel, A.V., Vale, R., Ruehle, S., Lefler, Y., and Branco, T. (2018). A synaptic threshold mechanism for computing escape decisions. Nature *558*, 590–594. https://doi.org/10.1038/s41586-018-0244-6.

45. Temizer, I., Donovan, J.C., Baier, H., and Semmelhack, J.L. (2015). A visual pathway for looming-evoked escape in larval zebrafish. Curr. Biol. *25*, 1823–1834. https://doi.org/10.1016/j.cub.2015.06.002.

46. Dunn, T.W., Gebhardt, C., Naumann, E.A., Riegler, C., Ahrens, M.B., Engert, F., and Del Bene, F. (2016). Neural circuits underlying visually evoked escapes in larval zebrafish. Neuron *89*, 613–628. https://doi.org/10.1016/j.neuron.2015.12.021.

47. Wullimann, M.F., Mokayes, N., Shainer, I., Kuehn, E., and Baier, H. (2024). Genoarchitectonics of the larval zebrafish diencephalon. J. Comp. Neurol. *532*, e25549. https://doi.org/10.1002/cne.25549.

48. Moini, J., and Piran, P. (2020). Diencephalon: thalamus and hypothalamus. In Functional and Clinical Neuroanatomy (Elsevier), pp. 267–292. https://doi.org/10.1016/B978-0-12-817424-1.00008-2.

49. Dan, C., Hulse, B.K., Kappagantula, R., Jayaraman, V., and Hermundstad, A.M. (2021). A neural circuit architecture for rapid behavioral flexibility in goal-directed navigation. Preprint at bioRxiv. https://doi.org/10.1101/2021.08.18.456004.

50. Zador, A.M. (2019). A critique of pure learning and what artificial neural networks can learn from animal brains. Nat. Commun. *10*, 3770. https://doi.org/10.1038/s41467-019-11786-6.

51. Wilson Alphonse, C.R., and Rajaretinam, R.K. (2022). Habituation and behavioural response of confinement-induced anxiety conditions in a zebrafish model. Appl. Biosci. *1*, 315–323. https://doi.org/10.3390/applbiosci1030020.

52. Tsai, H.-C., Zhang, F., Adamantidis, A., Stuber, G.D., Bonci, A., De Lecea, L., and Deisseroth, K. (2009). Phasic firing in dopaminergic neurons is sufficient for behavioral conditioning. Science *324*, 1080–1084. https://doi.org/10.1126/science.1168878.

53. LeDoux, J.E. (2000). Emotion circuits in the brain. Annu. Rev. Neurosci. *23*, 155–184. https://doi.org/10.1146/annurev.neuro.23.1.155.

54. Daw, N.D., Kakade, S., and Dayan, P. (2002). Opponent interactions between serotonin and dopamine. Neural Netw. *15*, 603–616. https://doi.org/10.1016/S0893-6080(02)00052-7.

55. Schweimer, J.V., and Ungless, M.A. (2010). Phasic responses in dorsal raphe serotonin neurons to noxious stimuli. Neuroscience *171*, 1209–1215. https://doi.org/10.1016/j.neuroscience.2010.09.058.

56. Uematsu, A., Tan, B.Z., Ycu, E.A., Cuevas, J.S., Koivumaa, J., Junyent, F., Kremer, E.J., Witten, I.B., Deisseroth, K., and Johansen, J.P. (2017). Modular organization of the brainstem noradrenaline system coordinates opposing learning states. Nat. Neurosci. *20*, 1602–1611. https://doi.org/10.1038/nn.4642.

57. Giustino, T.F., and Maren, S. (2018). Noradrenergic modulation of fear conditioning and extinction. Front. Behav. Neurosci. *12*, 43. https://doi.org/10.3389/fnbeh.2018.00043.

58. Inglis, F.M., and Moghaddam, B. (1999). Dopaminergic innervation of the amygdala is highly responsive to stress. J. Neurochem. *72*, 1088–1094. https://doi.org/10.1046/j.1471-4159.1999.0721088.x.

59. Joshua, M., Adler, A., Mitelman, R., Vaadia, E., and Bergman, H. (2008). Midbrain dopaminergic neurons and striatal cholinergic interneurons encode the difference between reward and aversive events at different epochs of probabilistic classical conditioning trials. J. Neurosci. *28*, 11673–11684. https://doi.org/10.1523/JNEUROSCI.3839-08.2008.

60. Tabor, K.M., Bergeron, S.A., Horstick, E.J., Jordan, D.C., Aho, V., Porkka-Heiskanen, T., Haspel, G., and Burgess, H.A. (2014). Direct activation of the Mauthner cell by electric field pulses drives ultrarapid escape responses. J. Neurophysiol. *112*, 834–844. https://doi.org/10.1152/jn.00228.2014.

61. Davison, J.M., Akitake, C.M., Goll, M.G., Rhee, J.M., Gosse, N., Baier, H., Halpern, M.E., Leach, S.D., and Parsons, M.J. (2007). Transactivation from Gal4-VP16 transgenic insertions for tissue-specific cell labeling and ablation in zebrafish. Dev. Biol. *304*, 811–824. https://doi.org/10.1016/j.ydbio.2007.01.033.

62. Yao, Y., Li, X., Zhang, B., Yin, C., Liu, Y., Chen, W., Zeng, S., and Du, J. (2016). Visual cue-discriminative dopaminergic control of visuomotor transformation and behavior selection. Neuron *89*, 598–612. https://doi.org/10.1016/j.neuron.2015.12.036.

63. Schnörr, S.J., Steenbergen, P.J., Richardson, M.K., and Champagne, D.L. (2012). Measuring thigmotaxis in larval zebrafish. Behav. Brain Res. *228*, 367–374. https://doi.org/10.1016/j.bbr.2011.12.016.

64. Bouchard, M.B., Voleti, V., Mendes, C.S., Lacefield, C., Grueber, W.B., Mann, R.S., Bruno, R.M., and Hillman, E.M.C. (2015). Swept confocally-aligned planar excitation (SCAPE) microscopy for high-speed volumetric imaging of behaving organisms. Nat. Photon. *9*, 113–119. https://doi.org/10.1038/nphoton.2014.323.

65. Voleti, V., Patel, K.B., Li, W., Perez Campos, C., Bharadwaj, S., Yu, H., Ford, C., Casper, M.J., Yan, R.W., Liang, W., et al. (2019). Real-time volumetric microscopy of in vivo dynamics and large-scale samples with SCAPE 2.0. Nat. Methods *16*, 1054–1062. https://doi.org/10.1038/s41592-019-0579-4.

66. Sutton, R.S., and Barto, A.G. (2018). Reinforcement Learning: an Introduction (MIT Press).

67. Randlett, O., Wee, C.L., Naumann, E.A., Nnaemeka, O., Schoppik, D., Fitzgerald, J.E., Portugues, R., Lacoste, A.M.B., Riegler, C., Engert, F., et al. (2015). Whole-brain activity mapping onto a zebrafish brain atlas. Nat. Methods *12*, 1039–1046. https://doi.org/10.1038/nmeth.3581.

68. Mu, Y., Bennett, D.V., Rubinov, M., Narayan, S., Yang, C.-T., Tanimoto, M., Mensh, B.D., Looger, L.L., and Ahrens, M.B. (2019). Glia accumulate evidence that actions are futile and suppress unsuccessful behavior. Cell *178*, 27–43.e19. https://doi.org/10.1016/j.cell.2019.05.050.

69. Suryanarayana, S.M., Robertson, B., Wallén, P., and Grillner, S. (2017). The lamprey pallium provides a blueprint of the mammalian layered cortex. Curr. Biol. *27*, 3264–3277.e5. https://doi.org/10.1016/j.cub.2017.09.034.

70. Frank, T., Mönig, N.R., Satou, C., Higashijima, S.I., and Friedrich, R.W. (2019). Associative conditioning remaps odor representations and modifies inhibition in a higher olfactory brain area. Nat. Neurosci. *22*, 1844–1856. https://doi.org/10.1038/s41593-019-0495-z.

71. Hikosaka, O., Sesack, S.R., Lecourtier, L., and Shepard, P.D. (2008). Habenula: crossroad between the basal ganglia and the limbic system. J. Neurosci. *28*, 11825–11829. https://doi.org/10.1523/JNEUROSCI.3463-08.2008.

72. Xu, C., Sun, Y., Cai, X., You, T., Zhao, H., Li, Y., and Zhao, H. (2018). Medial habenula-interpeduncular nucleus circuit contributes to anhedonia-like behavior in a rat model of depression. Front. Behav. Neurosci. *12*, 238. https://doi.org/10.3389/fnbeh.2018.00238.

73. Bartoszek, E.M., Ostenrath, A.M., Jetti, S.K., Serneels, B., Mutlu, A.K., Chau, K.T.P., and Yaksi, E. (2021). Ongoing habenular activity is driven by forebrain networks and modulated by olfactory stimuli. Curr. Biol. *31*, 3861–3874.e3. https://doi.org/10.1016/j.cub.2021.08.021.

74. Facciol, A., and Gerlai, R. (2020). Zebrafish shoaling, its behavioral and neurobiological mechanisms, and its alteration by embryonic alcohol exposure: a review. Front. Behav. Neurosci. *14*, 572175. https://doi.org/10.3389/fnbeh.2020.572175.

75. Adolph, K.E., and Franchak, J.M. (2017). The development of motor behavior. Wiley Interdiscip. Rev. Cogn. Sci. *8*, e1430. https://doi.org/10.1002/wcs.1430.

76. Altman, J., and Sudarshan, K. (1975). Postnatal development of locomotion in the laboratory rat. Anim. Behav. *23*, 896–920. https://doi.org/10.1016/0003-3472(75)90114-1.

77. Thornton, A. (2008). Variation in contributions to teaching by meerkats. Proc. Biol. Sci. *275*, 1745–1751. https://doi.org/10.1098/rspb.2008.0268.

78. Bray, J., Emery Thompson, M., Muller, M.N., Wrangham, R.W., and Machanda, Z.P. (2018). The development of feeding behavior in wild chimpanzees (*Pan troglodytes schweinfurthii*). Am. J. Phys. Anthropol. *165*, 34–46. https://doi.org/10.1002/ajpa.23325.

79. Hoppitt, W.J.E., Brown, G.R., Kendal, R., Rendell, L., Thornton, A., Webster, M.M., and Laland, K.N. (2008). Lessons from animal teaching. Trends Ecol. Evol. *23*, 486–493. https://doi.org/10.1016/j.tree.2008.05.008.

80. Seyfarth, R.M., and Cheney, D.L. (1986). Vocal development in vervet monkeys. Anim. Behav. *34*, 1640–1658. https://doi.org/10.1016/S0003-3472(86)80252-4.

81. Goldshtein, A., Harten, L., and Yovel, Y. (2022). Mother bats facilitate pup navigation learning. Curr. Biol. *32*, 350–360.e4. https://doi.org/10.1016/j.cub.2021.11.010.

82. Caro, T.M., and Hauser, M.D. (1992). Is there teaching in nonhuman animals? Q. Rev. Biol. *67*, 151–174. https://doi.org/10.1086/417553.

83. Chivers, D., Mirza, R., and Johnston, J. (2002). Learned recognition of heterospecific alarm cues enhances survival during encounters with predators. Behav. *139*, 929–938. https://doi.org/10.1163/156853902320387909.

84. Brown, G.E., and Magnavacca, G. (2003). Predator inspection behaviour in a characin fish: an interaction between chemical and visual information? Ethology *109*, 739–750. https://doi.org/10.1046/j.1439-0310.2003.00919.x.

85. Horn, M.E., Ferrari, M.C.O., and Chivers, D.P. (2019). Retention of learned predator recognition in embryonic and juvenile rainbow trout. Behav. Ecol. *30*, 1575–1582. https://doi.org/10.1093/beheco/arz116.

86. Herculano-Houzel, S. (2017). Numbers of neurons as biological correlates of cognitive capability. Curr. Opin. Behav. Sci. *16*, 1–7. https://doi.org/10.1016/j.cobeha.2017.02.004.

87. Sol, D., Olkowicz, S., Sayol, F., Kocourek, M., Zhang, Y., Marhounová, L., Osadnik, C., Corssmit, E., Garcia-Porta, J., Martin, T.E., et al. (2022). Neuron numbers link innovativeness with both absolute and relative brain size in birds. Nat. Ecol. Evol. *6*, 1381–1389. https://doi.org/10.1038/s41559-022-01815-x.

88. Ströckens, F., Neves, K., Kirchem, S., Schwab, C., Herculano-Houzel, S., and Güntürkün, O. (2022). High associative neuron numbers could drive cognitive performance in corvid species. J. Comp. Neurol. *530*, 1588–1605. https://doi.org/10.1002/cne.25298.

89. Harpaz, R., Nguyen, M.N., Bahl, A., and Engert, F. (2021). Precise visuomotor transformations underlying collective behavior in larval zebrafish. Nat. Commun. *12*, 6578. https://doi.org/10.1038/s41467-021-26748-0.

90. Spence, R., Gerlach, G., Lawrence, C., and Smith, C. (2008). The behaviour and ecology of the zebrafish, *Danio rerio*. Biol. Rev. Camb. Philos. Soc. *83*, 13–34. https://doi.org/10.1111/j.1469-185X.2007.00030.x.

91. Bures, J., Bermudez-Rattoni, F., and Yamamoto, T. (1998). Conditioned Taste Aversion (Oxford University Press). https://doi.org/10.1093/acprof:oso/9780198523475.001.0001.

92. Rosenberg, M., Zhang, T., Perona, P., and Meister, M. (2021). Mice in a labyrinth show rapid learning, sudden insight, and efficient exploration. eLife *10*, e66175. https://doi.org/10.7554/eLife.66175.

93. Weber, D., Richter, V., Rohwedder, A., Großjohann, A., and Thum, A.S. (2023). Learning and memory in drosophila larvae. Cold Spring Harb. Protoc. *2023*, 107863. https://doi.org/10.1101/pdb.top107863.

94. Zwaka, H., McGinnis, O.J., Pflitsch, P., Prabha, S., Mansinghka, V., Engert, F., and Bolton, A.D. (2022). Visual object detection biases escape trajectories following acoustic startle in larval zebrafish. Curr. Biol. *32*, 5116–5125.e3. https://doi.org/10.1016/j.cub.2022.10.050.

95. Bhattacharyya, K., McLean, D.L., and MacIver, M.A. (2017). Visual threat assessment and reticulospinal encoding of calibrated responses in larval zebrafish. Curr. Biol. *27*, 2751–2762.e6. https://doi.org/10.1016/j.cub.2017.08.012.

96. Lovett-Barron, M., Andalman, A.S., Allen, W.E., Vesuna, S., Kauvar, I., Burns, V.M., and Deisseroth, K. (2017). Ancestral circuits for the coordinated modulation of brain state. Cell *171*, 1411–1423.e17. https://doi.org/10.1016/j.cell.2017.10.021.

97. Uribe-Arias, A., Rozenblat, R., Vinepinsky, E., Marachlian, E., Kulkarni, A., Zada, D., Privat, M., Topsakalian, D., Charpy, S., Candat, V., et al. (2023). Radial astrocyte synchronization modulates the visual system during behavioral-state transitions. Neuron *111*, 4040–4057.e6. https://doi.org/10.1016/j.neuron.2023.09.022.

98. Duboué, E.R., Hong, E., Eldred, K.C., and Halpern, M.E. (2017). Left habenular activity attenuates fear responses in larval zebrafish. Curr. Biol. *27*, 2154–2162.e3. https://doi.org/10.1016/j.cub.2017.06.017.

99. Cherng, B.-W., Islam, T., Torigoe, M., Tsuboi, T., and Okamoto, H. (2020). The dorsal lateral habenula-interpeduncular nucleus pathway is essential for left-right-dependent decision making in zebrafish. Cell Rep. *32*, 108143. https://doi.org/10.1016/j.celrep.2020.108143.

100. Palieri, V., Paoli, E., Wu, Y.K., Haesemeyer, M., Grunwald Kadow, I.C.G., and Portugues, R. (2024). The preoptic area and dorsal habenula jointly support homeostatic navigation in larval zebrafish. Curr. Biol. *34*, 489–504.e7.

101. Tay, T.L., Ronneberger, O., Ryu, S., Nitschke, R., and Driever, W. (2011). Comprehensive catecholaminergic projectome analysis reveals single-neuron integration of zebrafish ascending and descending dopaminergic systems. Nat. Commun. *2*, 171. https://doi.org/10.1038/ncomms1171.

102. Braford, M.R., Jr. (1995). Comparative aspects of forebrain organization in the ray-finned fishes: touchstones or not? Brain Behav. Evol. *46*, 259–274. https://doi.org/10.1159/000113278.

103. Northcutt, R.G. (2006). Connections of the lateral and medial divisions of the goldfish telencephalic pallium. J. Comp. Neurol. *494*, 903–943. https://doi.org/10.1002/cne.20853.

104. Ganz, J., Kroehne, V., Freudenreich, D., Machate, A., Geffarth, M., Braasch, I., Kaslin, J., and Brand, M. (2014). Subdivisions of the adult zebrafish pallium based on molecular marker analysis. F1000Res *3*, 308. https://doi.org/10.12688/f1000research.5595.2.

105. Dejean, C., Courtin, J., Rozeske, R.R., Bonnet, M.C., Dousset, V., Michelet, T., and Herry, C. (2015). Neuronal circuits for fear expression and recovery: recent advances and potential therapeutic strategies.

Biol. Psychiatry *78*, 298–306. https://doi.org/10.1016/j.biopsych.2015.03.017.

106. Myers, K.M., and Davis, M. (2007). Mechanisms of fear extinction. Mol. Psychiatry *12*, 120–150. https://doi.org/10.1038/sj.mp.4001939.
107. Schulz, B., Fendt, M., and Schnitzler, H.U. (2002). Clonidine injections into the lateral nucleus of the amygdala block acquisition and expression of fear-potentiated startle. Eur. J. Neurosci. *15*, 151–157. https://doi.org/10.1046/j.0953-816x.2001.01831.x.
108. Tanaka, T., Yokoo, H., Mizoguchi, K., Yoshida, M., Tsuda, A., and Tanaka, M. (1991). Noradrenaline release in the rat amygdala is increased by stress: studies with intracerebral microdialysis. Brain Res. *544*, 174–176. https://doi.org/10.1016/0006-8993(91)90902-8.
109. McGaugh, J.L. (2000). Memory–a century of consolidation. Science *287*, 248–251. https://doi.org/10.1126/science.287.5451.248.
110. O'Donnell, J., Zeppenfeld, D., McConnell, E., Pena, S., and Nedergaard, M. (2012). Norepinephrine: A neuromodulator that boosts the function of multiple cell types to optimize CNS performance. Neurochem. Res. *37*, 2496–2512. https://doi.org/10.1007/s11064-012-0818-x.
111. Bergles, D.E., Doze, V.A., Madison, D.V., and Smith, S.J. (1996). Excitatory actions of norepinephrine on multiple classes of hippocampal CA1 interneurons. J. Neurosci. *16*, 572–585. https://doi.org/10.1523/JNEUROSCI.16-02-00572.1996.
112. Haas, H.L., and Rose, G.M. (1987). Noradrenaline blocks potassium conductance in rat dentate granule cells in vitro. Neurosci. Lett. *78*, 171–174. https://doi.org/10.1016/0304-3940(87)90628-8.
113. Wallace, M.L., Huang, K.W., Hochbaum, D., Hyun, M., Radeljic, G., and Sabatini, B.L. (2020). Anatomical and single-cell transcriptional profiling of the murine habenular complex. eLife *9*, e51271. https://doi.org/10.7554/eLife.51271.
114. Bussmann, J., and Schulte-Merker, S. (2011). Rapid BAC selection for tol2-mediated transgenesis in zebrafish. Development *138*, 4327–4332. https://doi.org/10.1242/dev.068080.
115. Asakawa, K., Suster, M.L., Mizusawa, K., Nagayoshi, S., Kotani, T., Urasaki, A., Kishimoto, Y., Hibi, M., and Kawakami, K. (2008). Genetic dissection of neural circuits by Tol2 transposon-mediated Gal4 gene and enhancer trapping in zebrafish. Proc. Natl. Acad. Sci. USA *105*, 1255–1260. https://doi.org/10.1073/pnas.0704963105.
116. Yang, E., Zwart, M.F., James, B., Rubinov, M., Wei, Z., Narayan, S., Vladimirov, N., Mensh, B.D., Fitzgerald, J.E., and Ahrens, M.B. (2022). A brainstem integrator for self-location memory and positional homeostasis in zebrafish. Cell *185*, 5011–5027.e20. https://doi.org/10.1016/j.cell.2022.11.022.
117. Yokogawa, T., Hannan, M.C., and Burgess, H.A. (2012). The dorsal raphe modulates sensory responsiveness during arousal in zebrafish. J. Neurosci. *32*, 15205–15215. https://doi.org/10.1523/JNEUROSCI.1019-12.2012.
118. Curado, S., Stainier, D.Y.R., and Anderson, R.M. (2008). Nitroreductase-mediated cell/tissue ablation in zebrafish: a spatially and temporally controlled ablation method with applications in developmental and regeneration studies. Nat. Protoc. *3*, 948–954. https://doi.org/10.1038/nprot.2008.58.
119. Kawashima, T., Zwart, M.F., Yang, C.-T., Mensh, B.D., and Ahrens, M.B. (2016). The serotonergic system tracks the outcomes of actions to mediate short-term motor learning. Cell *167*, 933–946.e20. https://doi.org/10.1016/j.cell.2016.09.055.
120. Bogovic, J.A., Hanslovsky, P., Wong, A., and Saalfeld, S. (2016). Robust registration of calcium images by learned contrast synthesis. In 2016 IEEE 13th International Symposium on Biomedical Imaging (ISBI), pp. 1123–1126. https://doi.org/10.1109/ISBI.2016.7493463.

Please cite this article in press as: Zocchi et al., Days-old zebrafish rapidly learn to recognize threatening agents through noradrenergic and forebrain circuits, Current Biology (2024), https://doi.org/10.1016/j.cub.2024.11.057

STAR★METHODS

KEY RESOURCES TABLE

REAGENT or RESOURCE	SOURCE	IDENTIFIER
Chemicals, peptides, and recombinant proteins		
Metronidazole	Sigma	Cat: M3761-5G; CAS: 443-48-1
Deposited data		
Source data	This paper	Mendeley Data doi: https://doi.org/10.17632/wkxwggvfbx.1
Experimental models: Organisms/strains		
Tg(elavl3:H2B-GCaMP7f)^{jf90}	Yang et al.[116]	N/A
Tg(UAS:GCaMP6f)^{jf46}	Mu et al.[104]	N/A
Tg(tph2:Gal4)^{y228}	Yokogawa et al.[117]	ZDB-ALT-121114-9
Tg(dat:Gal4)	Yao et al.[62]	N/A
Tg(UAS-E1B:NTR-mCherry)^{c264}	Davison et al.[61]	ZDB-ALT-070316-1
Tg(dbh:Gal4)	This paper	N/A
Software and algorithms		
FIJI	NIH Image	https://imagej.nih.gov/ij/
Adobe Illustrator	Adobe, San Jose, CA	https://www.adobe.com/products/illustrator.html
Custom code	This paper	Mendeley Data doi: https://doi.org/10.17632/wkxwggvfbx.1

EXPERIMENTAL MODEL DETAILS

Fish

All zebrafish larvae were reared at 14:10 light-dark cycles according to standard protocols at 28.5°C. Zebrafish were fed rotifers and used for experiments. Zebrafish sex cannot be determined until 3 weeks post-fertilization, so experimental animals' sex was unknown. Transgenic animals used in this study were:

- *Tg(elavl3:H2B-GCaMP7f)^{jf90}* from Yang et al.[116]
- *Tg(UAS:GCaMP6f)^{jf46}* from Mu et al.[68]
- *Tg(tph2:Gal4)* from Yokogawa et al.[117]
- *Tg(dat:Gal4)* from Yao et al.[62]
- *Tg(UAS-E1B:NTR-mCherry)^{c264}* from Davison et al.[61]
- *Tg(dbh:Gal4)* (This paper)

All experiments presented in this study were conducted according to the animal research guidelines from NIH and were approved by the Institutional Animal Care and Use Committee and Institutional Biosafety Committee of Janelia Research Campus.

METHOD DETAILS

Behavior – Setup

For the smaller, rectangular arena, the chamber was constructed by laser-cutting a 2.5 x 2 cm rectangle into a piece of opaque 5 mm thick acrylic, and sealing a glass coverslip to the bottom with molten parafilm. For the larger arena, the 6 cm diameter circular chamber was machined from a piece of IR transparent acrylic. An opaque diffusive screen was attached to the bottom of the chambers to mask out the apparatus below. For both assays, an infrared LED array, covered by a diffuser, provided illumination from below. A camera – Pike, F-032 for the smaller arena setup or FLIR BFS-U3-32S4C-C for the larger setup – equipped with a zoom lens (Computar M3Z1228C-MP) recorded the arena from above. The robot consisted of a stack of three-to-five 1 mm diameter, 1 mm height neodymium magnets, painted red, blue, or black, forming a 3-5 mm high cylinder (first4magnets F305 painted with Humbrol enamel paint). This magnetic robot was moved, remotely, via a second magnet (a stack of the same type of magnet) directly beneath the arena, which was glued to an acrylic platform just below the arena; the position of this second magnet was controlled by two linear stages (Zaber, X-LSQ150B) that moved the acrylic platform, and moved the magnet in the arena through magnetic attraction. The stages were controlled by the computer that received a visual feed of the fish and robot filmed from above. For a small subset of experiments in the smaller arena, the robot consisted of a bent glass rod similarly painted at the end (World Precision Instruments TW 150-3), controlled by the translation stages (fish learned simvolilarly with the magnetic robot and the small subset of experiments

Please cite this article in press as: Zocchi et al., Days-old zebrafish rapidly learn to recognize threatening agents through noradrenergic and forebrain circuits, Current Biology (2024), https://doi.org/10.1016/j.cub.2024.11.057

performed with the glass robot). For the robot recognition experiments, one robot was painted red, and the other blue. The identities of the aggressive and benign robots were switched across experiments, so that 50% of the time the aggressive robot was red and 50% of the time it was blue. The entire setup was enclosed in a box, with white light LEDs (Capetronix) glued to the roof to provide illumination for the fish. Custom Python software (available upon request and will be deposited to a repository) streamed frames from the camera (using a FireWire interface) at 100 frames per second, saved them to a video file, tracked the position of the fish, and controlled the linear stages.

Behavior - Analysis and Tracking

Real time tracking of fish position during the behavioral experiments was done using custom Python software utilizing the openCV package (opencv-python) (available upon request and will be deposited). The raw frames read from the camera were background subtracted, convolved with a Gaussian filter, binarized using a threshold, and then passed through a contour detector. Filtering by area, and sometimes aspect ratio, then allowed identification of the contour corresponding to the fish. The centroid of the 'blob' defined by the contour was used as the fish position. The fish positions were saved along with the raw video, and were used as the end points for linear stage movements during the training periods.

For quadrant occupancy calculations, a rectangular region of interest (ROI) was traced around the behavioral arena, and divided evenly into 4 rectangular quadrants. The occupancy of any given quadrant was then calculated as the number of time points the centroid of the fish was found to be within the quadrant divided by the total number of time points. Kernel density estimates for the occupancy data (histograms in Figures 1, 2, and 4) were generated from occupancies of the magnet quadrant or every other quadrant combined. A Gaussian kernel was used with bandwidth set using the Silverman method. Because occupancies are bounded on the unit interval with substantial density close to 0, we needed to account for probability density assigned outside the boundary [0,1] from data close to these limits. We used the reflection method – briefly, the dataset was reflected about the boundaries - 0 and 1 - and the density was estimated on this concatenated dataset. What is displayed in the figures is the portion of the fitted density within the unit interval, normalized to 1. For the occupancy time course analysis, the occupancy of a given quadrant was calculated in a 4-minute sliding window, with 1-minute steps (Figure 1E). To calculate speed, the magnitude of the vector connecting consecutive fish positions was divided by the time between the frames that generated those positions (Figures S1, S2, and S4). For display, the speed array was smoothed with a median filter, and the average speed in a sliding 30 s window (10 s bins), was plotted. Swim bout frequency was calculated by first identifying swim events as peaks in the filtered swim array using a peak detection algorithm (scipy.signal find_peaks) (Figures S1, S2, and S4). The number of swim events in a sliding 30 s window (10 s bins) were summed and divided by the window length to generate a peristimulus time histogram of swim bout frequency. Mixture models were fit using 3 (Figure S1) or 2 (Figure S2) Gaussian components on the difference in occupancy of the arena quadrant currently holding the magnet. Learner fish should display negative values for this quantity, on average, while non-learners should display non-negative values. Therefore, we constrained the models to have one component with negative mean (learners), and the other with non-negative mean (non-learners). The posterior probability for each data point belonging to different components of the model was calculated, and individual datapoints were clustered as belonging to either the learner or non-learner class based on whichever component yielded the highest probability. Three components were used for the data in Figure S1C because of the presence of a clear outlier (single point with a change in occupancy of 0.58). One of the three components accounted entirely for this outlier (red component in Figure S1C), leaving the other two components to account for the remainder of the data.

Behavior - Assays

Fish tested in the small arena variant of CRA (all figures except Figure S2) were screened for even swimming through the behavioral arena: only fish that spent at least 15% of their time in each of the four quadrants of the arena were used for CRA behavioral experiments (except for the forebrain aspiration experiments where low yield forced us to relax these conditions and use fish who spent at least 10% of their time in each quadrant). For the large, circular arena variant of CRA (Figure S2), a larger area to explore led to less uniform exploration on average, so the criteria used for inclusion in analysis was at least 10% time spent in each of the four quadrants pre-training. During pre- and post-training periods, the robot sat stationary in the middle of a single quadrant. These periods lasted 10 minutes except for the learning time course experiments (Figures 1E and S1H), where the post-training period lasted 30 min or consisted of multiple 10-minute periods separated by an hour each, respectively. Training in CRA consisted of robot motion, at 7-10 mm/s, broken into alternating 3 s chase sequences and 6 s periods of random motion. During chase, the robot was moved to the current calculated fish centroid position in real time, moving along a straight line connecting the robot's current position to its target position. Speed was constant throughout motion (7-10 mm/s, depending on the experiment). Random motion was achieved by drawing positions from a uniform distribution. The distribution was bounded so that the robot moved within a $\sim$1 cm square in the center of the arena. Training consisting of alternating chase and random motion was repeated 20-27 times for a duration of between 3 and 4.5 minutes (60-90 seconds of chase). For the time course experiments of Figure S1H, two such training periods were used: one in between the pre- and post-training periods, and one immediately after the post-training period. Training in the larger circular arena was 1.5 minutes with 50% chase and 50% random motion (45 seconds of chase). It was important to break up the chases into short sequences because we found prolonged chases (longer than 5 s) would often result in fish freezing, and becoming unresponsive. For the general fear response control, training consisted of removing the fish from the arena, placing them in a small petri dish, and swirling the dish around for 135-225 s, before replacing the fish in the behavior chamber. In the robot recognition experiments, the benign robot remained immobile in a single quadrant, and an exclusion zone was defined around it which the aggressive robot could not

Please cite this article in press as: Zocchi et al., Days-old zebrafish rapidly learn to recognize threatening agents through noradrenergic and forebrain circuits, Current Biology (2024), https://doi.org/10.1016/j.cub.2024.11.057

enter during training, to prevent the robots (which were both magnets) from sticking to each other. For random motion variants of the assay, the robot moved at 1mm/s, at random, in a single quadrant of the arena for about 3 minutes. In the embedded robot assay, fish were allowed to swim freely in the presence of the immobile magnet (pre-training) for 10 minutes. For training, the fish were embedded in agarose with their heads free and the robot was let to approach the fish in a straight line, sit in front of it for 30s, and then retreat to mirror the assay used for SCAPE imaging. The fish was in closed loop control of the robot such that every time the fish flicked its tail, the robot would immediately retreat away from the fish, approximating the effect of freely-swimming avoidance maneuvers. The training lasted 10 minutes after which the fish was released from the agar and allowed to swim freely in the presence of the immobile robot (post-training) for 10 minutes.

Ablations

Ablations of the forebrain were performed using vacuum aspiration.[68] Larvae were anesthetized in tricaine, and mounted in agarose, dorsal side up, in the lid of a small petri dish. A window was cut into the agarose to expose the head. Glass pipettes with ~30 μm, and ~60 μm diameter were pulled from borosilicate glass capillary tubes (WPI). A 30 μm pipette was used to puncture a hole in the head directly above the forebrain, and the incision was then enlarged with a 60 μm diameter pipette to expose the brain. Another 30 μm pipette was fire polished, connected to a vacuum line, then used to aspirate the forebrain. The entire procedure was done under a wide-field dissecting microscope. Typically, aspirations were done starting from the habenula, which were clearly visible under the dissecting microscope, and moving rostrally. This resulted in the complete removal/destruction of the telencephalon, most of the habenula, and potentially some rostral portions of the thalamus and hypothalamus. Afterwards, fish were released from the agar, and placed back in their home dish for recovery. They were subsequently tested in the behavioral assay 2-5 days later. Controls consisted either of fish from the same clutch as ablated fish, or non-clutch mates who were anesthetized and mounted in agar in the same way as the ablated condition. The control data shown in Figures 4C and 4I, is an aggregate of these two controls.

Habenula ablations were done with a 2-photon laser. Larvae expressing nucleus-targeted GCaMP7f pan-neuronally, *Tg(elavl3:H2B-GCaMP7f)*, were mounted in agarose in the lid of a small Petri dish. The fish were placed under a confocal microscope (Zeiss, LSM980) equipped with a 2-photon laser excitation arm. We identified the habenulae using the pan-neuronal GCaMP signal, and then photobleached blocks of ~10-15 cells at a time with brief periods (~0.5 - 1s) of high power 2P irradiation. Cell destruction was clear under the confocal as fluorescence disappeared. Fish were released after the procedure, returned to their home dish for recovery, and tested 2-5 days later. For controls, we ablated the olfactory epithelium in the same way described above. Both the habenulae and olfactory epithelium were readily recognizable, and visually separable from surrounding regions.

Chemogenetic lesions of neuromodulatory circuits were done using the nitroreductase system.[118,119] Cell specific promoters drove expression of Gal4, while nitroreductase was under UAS control. The lesioned conditions were fish expressing both transgenes and incubated overnight in 10 mM metronidazole to induce ablations. Fish were tested in the behavioral assays after a 1-3 day recovery. Controls contained a single of the two transgenes and were also incubated in metronidazole overnight.

Imaging - Setup and Robot Stimuli

A custom built swept confocally aligned planar excitation (SCAPE) microscope[64,65] was used to image whole brain calcium activity at 1.3 - 1.5 volumes per second in a single-objective, upright geometry. An sCMOS camera (Andor, Zyla 4.2) with Nikon tube lens (Nikon 50 mm f/1.4 AF D) recorded oblique-plane images, and excitation was provided by a 488 nm laser (Coherent, Obis 488). Fish were paralyzed and mounted in agarose as described before,[116] with their heads exposed. A separate camera (FLIR BFS-U3-16S2M-CS) imaged the fish, robot, and imaging chamber from below under infrared illumination provided by an IR LED (ThorLabs, M850L3). A red LED (Mightex) provided illumination onto the imaging chamber for the fish to be able to see, while not corrupting the calcium imaging signals. A pair of linear stages (TOAUTO, T0601-50) moved the robot around the imaging chamber. The robot entered the chamber from above (as with the glass pipettes used in the free swimming assay), and consisted of three 1mm diameter, 1mm height, disc magnets stacked on top of each other (first4magnets, F305) painted red, and glued onto the end of a syringe needle, allowing it to be attached to an arm mounted onto the linear stages. The stepper motors of the stages were controlled using an Arduino (Arduino Uno Rev3), and a custom Python script (will be provided on request and uploaded to GitHub).

Robot motion stimuli consisted of an approach in a straight line towards the fish lasting 1.5 s, a 30 s 'sit' period where the robot sat approximately 0.75 mm in front of the fish offset by half a millimeter to the left, and a retreat lasting 1.5 s. This was repeated 3 times with 30 s breaks in between stimuli. The speed of the robot was between 1-2 mm/s to allow time to capture both the approach and sit portions in the brain imaging.

Imaging - Processing and Analysis

Images projected onto the camera chip from the SCAPE system are of an oblique section through the imaged object and so raw image volumes are skewed. We de-skewed the volumes by applying an affine transform. For analysis of imaging data across brain regions, the volumes were processed using a non-negative matrix factorization, cell segmentation pipeline.[68] In the Figure 3 traces, $\Delta F/F$ was calculated as $(F - F_0)/F_0$, where F_0 represents (fluorescence_readout – camera_baseline) averaged over 10 seconds prior to robot movement. In the Figures 3D–3F voxel heatmaps, F_0 represents fluorescence_readout averaged over 10 seconds prior to robot movement (without camera baseline subtracted to avoid division by small numbers due to pixel noise). Maximum intensity projections were thresholded at 25% of the max. pixel intensity for approach and sit; and at 25% of the average max. pixel intensity between approach and sit for the premotion map. Functional volumes were registered to the Z-Brain atlas[67] using the BigWarp and

Please cite this article in press as: Zocchi et al., Days-old zebrafish rapidly learn to recognize threatening agents through noradrenergic and forebrain circuits, Current Biology (2024), https://doi.org/10.1016/j.cub.2024.11.057

BigStream software packages[120] (https://github.com/JaneliaSciComp/bigstream). Masks from Z-Brain were used to define different brain regions used in the imaging analysis. Latency to peaks were calculated as the time from robot motion onset to the peak of single unit responses. Kernel density estimates were computed using Gaussian kernels and bandwidths chosen using the Silverman method. Cell response rasters were ordered by the center of mass of the traces. This was done by filtering each trace with a median filter, setting negative values to zero, and then calculating the centroid of this processed trace. For the LC response dynamics variability analysis, we calculated the average ΔF/F of each trials' normalized LC response (averaged over every LC neuron) over a 15 second period following onset of the stimulus. This yielded 21 LC early response levels (one for each trial). These values were clustered using k-means clustering with 2 clusters, and trials were classified as either LC sustained, or LC transient. Average responses across different regions between these trial types were then generated for comparison in the figures. Heatmaps in Figures 3E and 3F were thresholded at 20% of the maximum pixel value (E,F), such that only pixels with values above this threshold were displayed. The heatmap of Figure 3D was also thresholded using the average of the thresholds in E and F.

QUANTIFICATION AND STATISTICAL ANALYSIS

A detailed summary of all statistical tests is provided in Table S1. Sample sizes were not predetermined using a power analysis. The experimenter was not masked to experimental condition or genotype during data collection and analysis. Error bars in figures are standard error of the mean (SEM). Statistics were computed using the SciPy Stats package. Comparisons noted as ''not significant'' (n.s.) were not significant at a level of α=0.05. The specific statistical test used for each comparison is reported in the figure legends and Table S1.